AD-A057 255 PURDUE UNIV LAFAYETTE IND SCHOOL OF ELECTRICAL ENGI--ETC F/G 9/5
PERFORMANCE EVALUATION OF SIMPLE HF ANTENNA SYSTEMS.(U)
MAR 78 C L CHEN, W L WEEKS F19628-76-C-0086
UNCLASSIFIED SCIENTIFIC-2 RADC-TR-78-65 NL

1 OF 1
AD A057 255

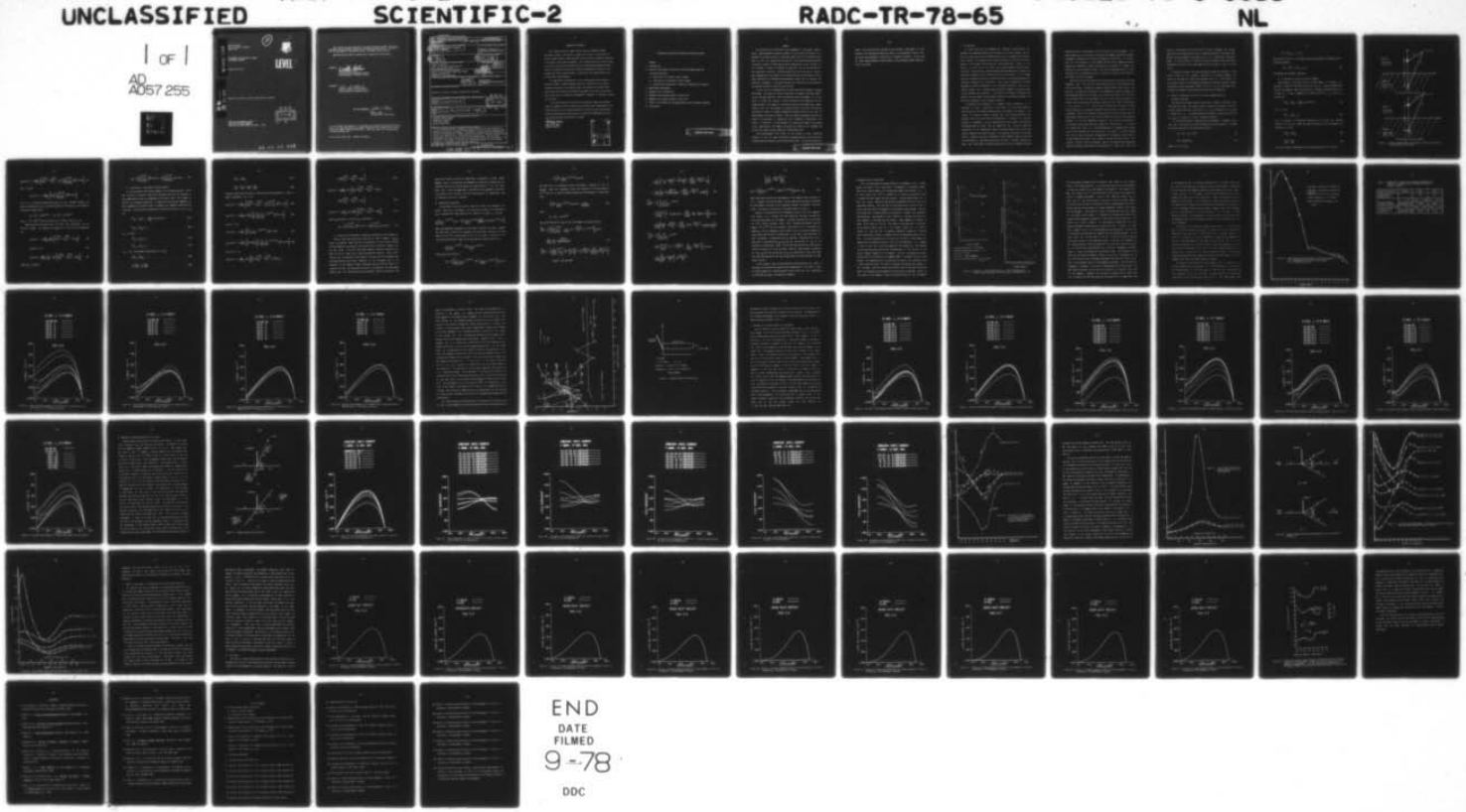

END
DATE FILMED
9-78
DDC

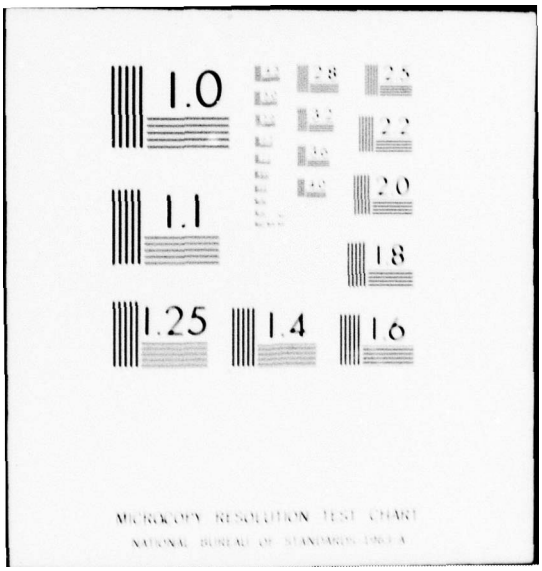
1.0
1.1
1.25
1.4
1.6
2.0
2.2
2.5
MICROCOPY RESOLUTION TEST CHART
NATIONAL BUREAU OF STANDARDS 1963-A

(11)

RADC-TR-78-65
Interim Technical Report
March 1978

PERFORMANCE EVALUATION OF SIMPLE HF ANTENNA SYSTEMS

LEVEL II

Purdue University

Approved for public release; distribution unlimited

ROME AIR DEVELOPMENT CENTER
AIR FORCE SYSTEMS COMMAND
GRIFFISS AIR FORCE BASE, NEW YORK 13441

This report has been reviewed by the RADC Information Office (OI) and is releasable to the National Technical Information Service (NTIS). At NTIS it will be releasable to the general public, including foreign nations.

RADC-TR-78-65 has been reviewed and is approved for publication.

APPROVED: Walter Rotman

WALTER ROTMAN, Chief
Antennas and RF Components Branch
Electromagnetic Sciences Division

APPROVED: Allan C. Schell

ALLAN C. SCHELL, Acting Chief
Electromagnetic Sciences Division

FOR THE COMMANDER: John P. Huss

JOHN P. HUSS
Acting Chief, Plans Office

If your address has changed or if you wish to be removed from the RADC mailing list, or if the addressee is no longer employed by your organization, please notify ESD (EEA), Hanscom AFB MA 01731. This will assist us in maintaining a current mailing list.

Do not return this copy. Retain or destroy.

UNCLASSIFIED

SECURITY CLASSIFICATION OF THIS PAGE (When Data Entered)

REPORT DOCUMENTATION PAGE	READ INSTRUCTIONS BEFORE COMPLETING FORM
1. REPORT NUMBER: RADC-TR-78-65	2. GOVT ACCESSION NO. / 3. RECIPIENT'S CATALOG NUMBER
4. TITLE (and Subtitle): PERFORMANCE EVALUATION OF SIMPLE HF ANTENNA SYSTEMS	5. TYPE OF REPORT & PERIOD COVERED: Scientific Report No. 2
	6. PERFORMING ORG. REPORT NUMBER: N/A
7. AUTHOR(s): C. L. Chen, W. L. Weeks	8. CONTRACT OR GRANT NUMBER(s): F19628-76-C-0086
9. PERFORMING ORGANIZATION NAME AND ADDRESS: Purdue University, School of Electrical Engineering, West Lafayette IN 47907	10. PROGRAM ELEMENT, PROJECT, TASK AREA & WORK UNIT NUMBERS: 61102F, 2305J428, J4
11. CONTROLLING OFFICE NAME AND ADDRESS: Deputy for Electronic Technology (RADC), Hanscom AFB MA 01731, Monitor/C.J. Drane/EEA	12. REPORT DATE: March 1978
	13. NUMBER OF PAGES: 74
14. MONITORING AGENCY NAME & ADDRESS (if different from Controlling Office): 74p.	15. SECURITY CLASS. (of this report): UNCLASSIFIED
	15a. DECLASSIFICATION/DOWNGRADING SCHEDULE: N/A

16. DISTRIBUTION STATEMENT (of this Report)

Approved for public release; distribution unlimited.

17. DISTRIBUTION STATEMENT (of the abstract entered in Block 20, if different from Report): Scientific-2

DDC RECEIVED AUG 9 1978 B

18. SUPPLEMENTARY NOTES: Interim technical rept.

19. KEY WORDS (Continue on reverse side if necessary and identify by block number)

Antenna Ground Systems
Sommerfeld Integrals
Field Enhancement
Front-to-Back Ratio

20. ABSTRACT (Continue on reverse side if necessary and identify by block number)

An extensive method of moments program (WF-LLL2B) has been modified to evaluate the effects of ground screen systems on the low angle radiation from vertically polarized HF antennas. Theoretical consideration was presented to justify the modification. The revised code was used to evaluate the HF antennas with ground screens of one, three and four ground wires. The low angle enhancement and front-to-back ratio of each ground screen were calculated. The influence of the height of back screen reflecting screens on the low angle radiation of broadside arrays was also studied.

DD FORM 1 JAN 73 1473 EDITION OF 1 NOV 65 IS OBSOLETE

UNCLASSIFIED

SECURITY CLASSIFICATION OF THIS PAGE (When Data Entered)

292 000 78 07 24 040

EVALUATION STATEMENT

This second scientific report under contract F19628-76-C-0086 describes in detail the results of analytical studies of the effects of ground screen and back screen designs on the low angle radiation properties of vertically polarized HF antennas. The ultimate purpose of these studies has been to provide the technical basis for developing engineering procedures for estimating the most cost-effective geometrical designs of such screens for specific applications in long-range, OTH communications and surveillance radar antennas.

The computations performed for these investigations were based on a method of moments computer program previously prepared at the Lawrence Livermore Laboratory, but modified under this contract to handle those cases where both antenna and screen wire elements are close to the earth and to each other. Evaluation of Sommerfeld integrals is involved in these calculations.

It was established that ground wires extending toward the backward direction generally tend to depreciate low-angle signal enhancement in the forward direction, with maximum depreciation occuring when these ground wires are approximately quarter-wave in length, but backscreens are most cost effective when quarter-wave in height.

Charles J. Drane

CHARLES J. DRANE
Contract Monitor

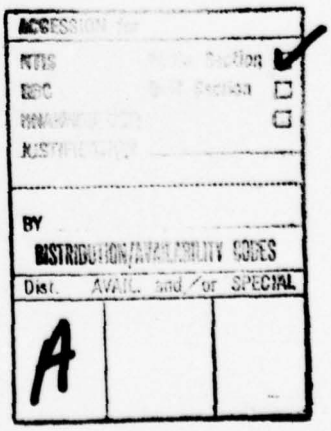

Performance Evaluation of Simple HF Antennas Systems

Summary

For the effective utilization of the ionosphere in long range communication systems between terminals located at the surface of the earth, it is desirable to radiate vertically polarized signals that are as strong as possible at the low angles near the horizon. Wire ground screens have been proposed as a means of enhancing the earth conductivity in the vicinity of the antennas in order to eliminate or reduce the "null at the horizon" effect observed in practice. The main objective of this work was to investigate systematically the effects of horizontal ground wire systems on the low angle radiation of HF antennas having moderate gains and to develop engineering procedures to estimate the most cost effective size and shape of such ground screens for specific applications.

To carry out the investigation, an extensive method of moments program (WF-LLL2B), previously written by researchers of Lawrence Livermore Laboratories, has been modified. With this modified code (WF-LLL2BP), it is possible to study the effects of thin, horizontal wires essentially at the ground surface. Our numerical calculation, based on WF-LLL2BP code, demonstrated that the distribution of induced current on the thin wires may be described in terms of a complex propagation constant, which in turn may be approximated by Coleman's formula. Once the complex propagation constant is known, it can be used in conjunction with elementary transmission line theory to establish a crude estimate for the desired length of the ground wires. Specifically, the lengths of ground wires should be so designed as to draw the return current toward the forward direction.

Also investigated is the effect of the height of back reflecting screens on the low angle radiation of broadside arrays, with the hope of reducing and optimizing the reflecting screen sizes. In the array type stu-

died, it was found that the increase of the low-angle enhancement by back screens of 3/4 wavelength height over that of 1/4 wavelength is small (5%), and resulting enhancement is sensitive to frequency variation. In this case at least, added expense of back screens of 3/4 wavelength height seems difficult to justify.

1. Introduction

It is well known that the impedance and radiation characteristics of antennas are affected greatly by the presence of an actual ground. The effect of a lossy ground can be demonstrated vividly by comparing the vertical field pattern of a monopole over a perfect ground with that over an actual ground. In the former case the vertical field pattern has a peak at the horizon ($\theta = 90°$) while the latter has a sharp minimum in that direction [1,2,3,4]. Ground wires or ground screens have been employed to improve the radiation resistance and the radiation patterns of antennas. It is a common practice to extend a ground wire system the order of a wavelength beyond the radiating antennas in all directions. This is quite reasonable for systems designed to radiate isotropically in all azimuthal directions. But for antennas systems with a moderate gain, perfectly symmetrical ground screens are not necessary nor economical. This study is an attempt to determine the optimal size and shapes of the ground screens for such antenna systems, with particular emphasis on the low-angle radiation.

To determine the radiation of an antenna system accurately, it is necessary to have a quantitative description of the current induced on various parts of the antenna system and the surrounding environment. Obviously for antenna systems situated near the air-earth interface, the presence of the lossy earth must be accounted for. Although the classical problem of elementary sources operating near the air-earth interface was formulated some sixty years ago by Sommerfeld [5], extensive numerical evaluation of the Sommerfeld integrals has been possible only since large digital computers have been available. The numerical evaluation of the Sommerfeld integrals has been incorporated in many computer codes to calculate the performance of radiating systems near the earth. A general purpose computer code (WF-LLL2B) written by Lager and Lytle [6] is probably the most

extensive one and is applicable to wire structures of various shapes. This code divides the wire structures into many wire segments and uses the method of moments to determine the current distribution on the wires. In calculating the self-impedance of each segment and the mutual impedances between segments the Sommerfeld integral expressions are evaluated by methods appropriate to the distances involved. The resulting impedance matrix is then converted into a system matrix which is inverted to solve for the current at the center of each wire segment.

Once the current distribution on the wire structure is known, the input impedance, near field and far field characteristics of the antenna system can be calculated. Although the computer code WF-LLL2B is quite useful and powerful, the numerical evaluation of the Sommerfeld integrals becomes very time consuming when wire structures very close to the ground are involved, say less than 1/30 of the wavelength. But for the HF antenna systems of interest, the wires making up the ground screens are very close to the ground, if not actually in it. Since our main interest was the effect of these ground systems on the radiation characteristics, we had to modify the WF-LLL2B code. Most of the features of WF-LLL2B were retained, except that the approximate expressions for the fields are used to alleviate the convergence problems of the exact Sommerfeld integrals. This report gives the details of the modifications made and their theoretical justification. To present the theoretical basis for the approximations, it is appropriate to start with a brief discussion of the fields due to an electric current element near the air-earth interface, although much of the material can be found in various books [3,4,5,7,8]. This is done in the next section so that a consistent notation may be introduced. Most of the notation and conventions used in the report are identical to those given by Lager and Lytle [6].

However a time-harmonic field of the $e^{+j\omega t}$ is used throughout the present report and this necessitates the use of Hankel functions of the second kind, $H_n^{(2)}(x)$, and the change of the branch cuts of the square-root functions. Except in the discussion in connection with the length of the wires, where both meters and feet will be used, MKS units will be used in rest of this report.

The modified computer code has been used to study the effects of the ground screens on the low-angle radiation of HF antenna systems. The results of the numerical study are presented in Sec. 4-7. The influence of the ground screens on the impedance properties of antennas has been studied extensively by Wait and others [9,10], and will not be discussed here, although the computer code employed also gives this information.

2. Electric Fields due to an Electric Current element above the Air-Earth Interface

We choose a coordinate system in which the air-earth interface coincides with z=0 plane. The region (region 1) below the interface is the lossy earth characterized by a permittivity $\epsilon_1 = \epsilon_r \epsilon_0$, permeability $\mu_1 = \mu_0$ and a conductivity σ_1. The space above the interface is taken to be air with $\epsilon_2 = \epsilon_0$, $\mu_2 = \mu_0$ and $\sigma_2 = 0$, and is labeled as region 2.

It is well-known that in dealing with electromagnetic problems involving two or more media, the Hertz potential vectors are helpful. In terms of the Hertz vecctor $\vec{\pi}$, the fields are given by

$$\vec{E}_i = \nabla(\nabla \cdot \vec{\pi}_i) + k_i^2 \vec{\pi}_i \tag{1}$$

$$\vec{B}_i = j(k_i^2/\omega)\nabla \times \vec{\pi}_i \tag{2}$$

where i = 1 or 2 and,

$$k_i^2 = \omega^2 \mu_i (\epsilon_i - j\,\sigma_i/\omega)$$

and the Hertz vector $\vec{\pi}_i$ is related to the current density $\vec{J}$ through the differential equation

$$\nabla^2 \vec{\pi}_i + k_i^2 \vec{\pi}_i = -\vec{J}/(\sigma_i + j\omega\epsilon_i) \tag{3}$$

and appropriate boundary conditions.

a) Fields due to a Vertical Current Element:

Now consider a z-directed electric current element $I\ell$ situated at a distance h above the interface as shown in Fig. 1a. It may be demonstrated that for the geometry under consideration all boundary conditions may be satisfied by a single component of the Hertz vector $\vec{\pi}_i = \pi_{iz}\,\hat{z}$, and π_{iz} is solved from

$$\nabla^2 \pi_{2z} + k_2^2 \pi_{2z} = -\frac{I\ell}{j\omega\epsilon_2}\,\delta(x)\delta(y)\delta(z-h) \tag{4a}$$

for $z > 0$, and

$$\nabla^2 \pi_{1z} + k_1^2 \pi_{1z} = 0 \tag{4b}$$

for $z < 0$, subject to the boundary conditions at $z = 0$, and the radiation condition at infinity. Under the restriction that $h \neq 0$, the boundary conditions at $z = 0$ are

$$k_1^2 \pi_{1z} = k_2^2 \pi_{2z} \tag{5a}$$

$$\frac{\partial \pi_{1z}}{\partial z} = \frac{\partial \pi_{2z}}{\partial z} \tag{5b}$$

In terms of Hankel transforms, the solutions may be cast in the form

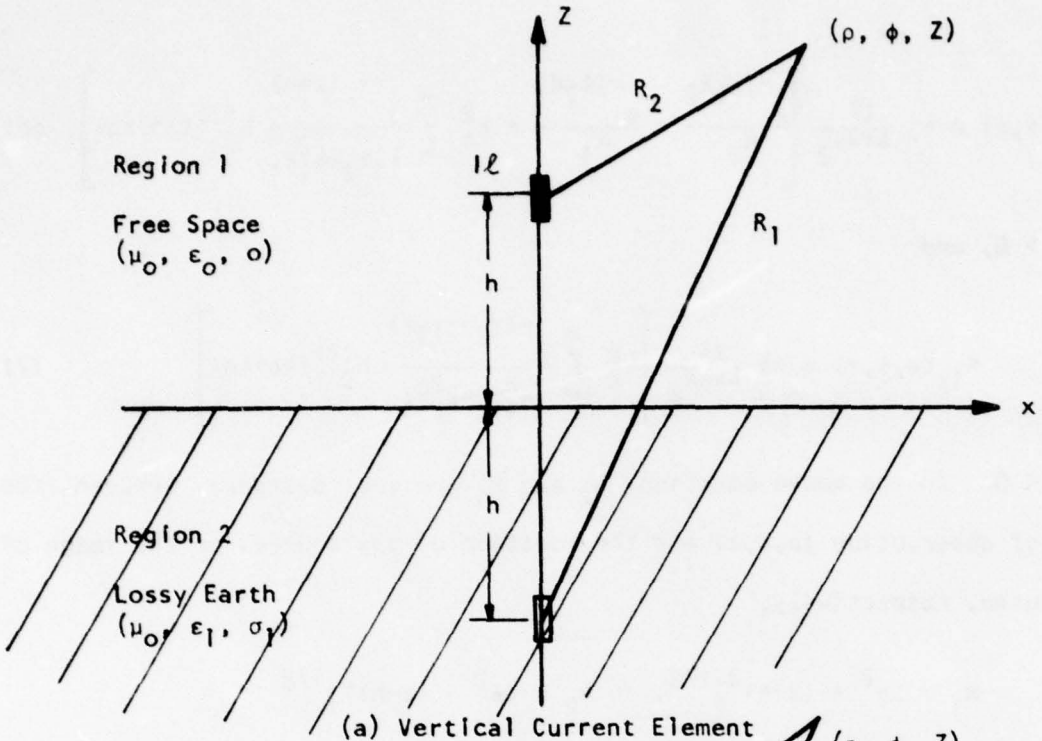

(a) Vertical Current Element

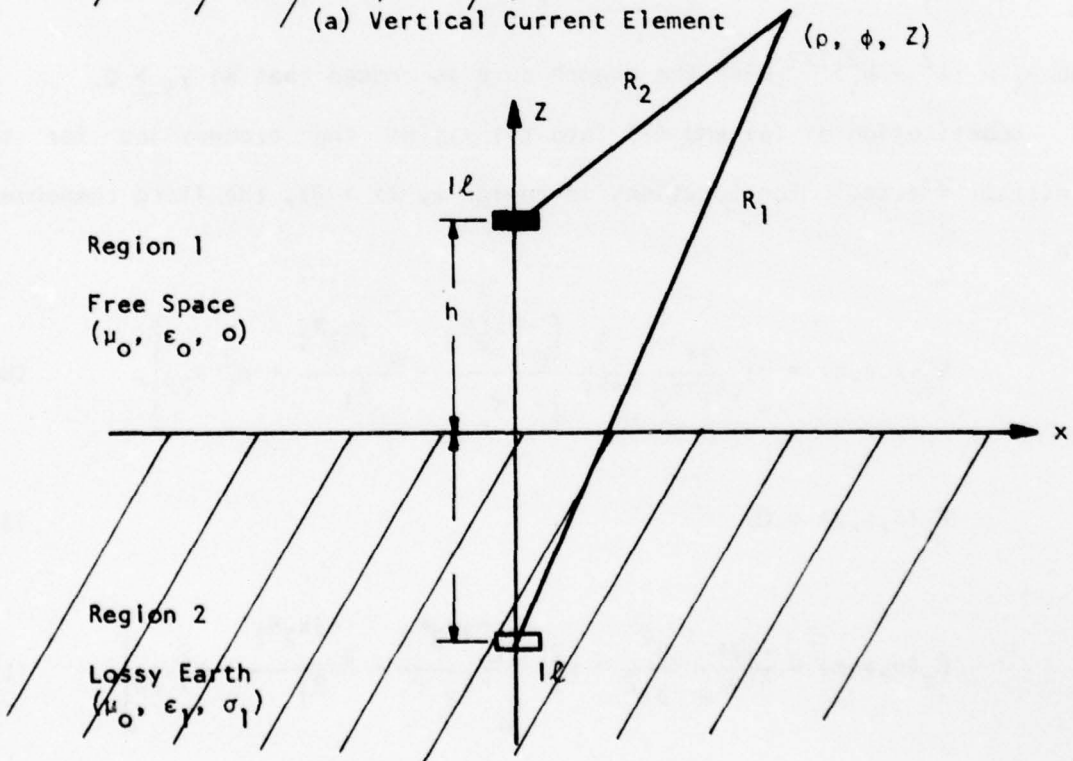

(b) Horizontal Current Element

Figure 1. Current Elements Above a Flat Earth a) Vertical Current and b) Horizontal Current Element

$$\pi_{2z}(\rho,\phi,z) = -j\frac{I\ell}{4\pi\omega\epsilon_2}\left[\frac{e^{-jk_2R_2}}{R_2} - \frac{e^{-jk_2R_1}}{R_1} + k_1^2\int_0^\infty \frac{e^{-\gamma_2(z+h)}}{k_1^2\gamma_2+k_2^2\gamma_1} H_0^{(2)}(\lambda\rho)\lambda d\lambda\right] \quad (6)$$

for $z > 0$, and

$$\pi_{1z}(\rho,\phi,z) = -j\frac{I\ell}{4\pi\omega\epsilon_2}\left[k_2^2\int_0^\infty \frac{e^{-(\gamma_2 h-\gamma_1 z)}}{k_1^2\gamma_2+k_2^2\gamma_1} H_0^{(2)}(\lambda\rho)\lambda d\lambda\right] \quad (7)$$

for $z < 0$. In the above equations R_2 and R_1 are the distance between the point of observation (ρ,ϕ,z) and the location of the source, or the image of the source, respectively,

$$R_1 = [\rho^2 + (z+h)^2]^{1/2}, \qquad R_2 = [\rho^2 + (z-h)^2]^{1/2}$$

and $\gamma_i = (\lambda^2 - k_i^2)^{1/2}$ with the branch cuts so chosen that Re $\gamma_i \geq 0$.

Substitution of (6) and (7) into (1) yields the expressions for the electric fields. For locations in region 2, $(z > 0)$, the field components are

$$E_\rho(\rho,\phi,z) = -j\frac{I\ell}{4\pi\omega\epsilon_2}\frac{\partial^2}{\partial\rho\partial z}\left[\frac{e^{-jk_2R_2}}{R_2} - \frac{e^{-jk_2R_1}}{R_1} + k_1^2 V_{22}\right], \quad (8a)$$

$$E_\phi(\rho,\phi,z) = 0, \quad (8b)$$

$$E_z(\rho,\phi,z) = \frac{-jI\ell}{4\pi\omega\epsilon_2}\left(\frac{\partial^2}{\partial z^2} + k_2^2\right)\left[\frac{e^{-jk_2R_2}}{R_2} - \frac{e^{-jk_2R_1}}{R_1} + k_1^2 V_{22}\right], \quad (8c)$$

where V_{22} is given by

$$V_{22} = \int_{-\infty}^{\infty} \frac{e^{-\gamma_2(h+z)}}{k_1^2\gamma_2+k_2^2\gamma_1} H_0^{(2)}(\lambda\rho)\lambda d\lambda = 2\int_0^{\infty} \frac{e^{-\gamma_2(h+z)}}{k_1^2\gamma_2+k_2^2\gamma_1} J_0(\lambda\rho)\lambda d\lambda, \qquad (9)$$

b) Fields due to a Horizontal Current Element:

For the case where the current element $I\ell$ is oriented along the x-axis and located at a distance h above the interface (Fig. 1b), the situation is more complicated in that two components of the Hertz vector are needed to satisfy the boundary conditions. In addition to the obvious component π_x, the z-component of the Hertz vector is needed if all boundary conditions are to be met. The differential equations for the Hertz vector $\vec{\pi}_i = \pi_{ix}\hat{x} + \pi_{iz}\hat{z}$ are

$$\nabla^2\pi_{2x} + k_2^2\pi_{2x} = -\frac{I\ell}{j\omega\epsilon_2}\delta(x)\delta(y)\delta(z-h) \qquad (10a)$$

$$\nabla^2\pi_{2z} + k_2^2\pi_{2z} = 0 \qquad (10b)$$

for $z > 0$ and

$$\nabla^2\pi_{1x} + k_1^2\pi_{1x} = 0 \qquad (11a)$$

$$\nabla^2\pi_{1z} + k_1^2\pi_{1z} = 0 \qquad (11b)$$

for $z < 0$. The boundary conditions at $z = 0$ are

$$k_1^2\pi_{1x} = k_2^2\pi_{2x} \qquad (12a)$$

$$k_1^2\frac{\partial\pi_{1x}}{\partial z} = k_2^2\frac{\partial\pi_{2x}}{\partial z} \qquad (12b)$$

$$k_1^2 \pi_{1x} = k_2^2 \pi_{2x} \tag{12c}$$

$$\frac{\partial \pi_{1x}}{\partial x} + \frac{\partial \pi_{1z}}{\partial z} = \frac{\partial \pi_{2x}}{\partial x} + \frac{\partial \pi_{2z}}{\partial z} \tag{12d}$$

The Hertz vector and the electric fields can also be expressed in terms of Hankel transforms. For $z > 0$,

$$\pi_{2x}(\rho,\phi,z) = -j \frac{I\ell}{4\pi\omega\varepsilon_2} \left[\frac{e^{-jk_2R_2}}{R_2} - \frac{e^{-jk_2R_1}}{R_1} + \int_{-\infty}^{\infty} \frac{e^{-\gamma_2(z+h)}}{\gamma_1 + \gamma_2} H_0^{(2)}(\lambda\rho)\lambda d\lambda \right] \tag{13a}$$

$$\pi_{2z}(\rho,\phi,z) = -j \frac{I\ell}{4\pi\omega\varepsilon_2} \cos\phi \frac{\partial}{\partial\rho} \left[\int_{-\infty}^{\infty} \frac{\gamma_2 - \gamma_1}{\gamma_2 k_1^2 + \gamma_1 k_2^2} e^{-\gamma_2(z+h)} H_0^{(2)}(\lambda\rho)\lambda d\lambda \right] \tag{13b}$$

and for $z < 0$,

$$\pi_{1x}(\rho,\phi,z) = -j \frac{I\ell}{4\pi\omega\varepsilon_2} \frac{k_2^2}{k_1^2} \int_{-\infty}^{\infty} \frac{1}{\gamma_1+\gamma_2} e^{(-\gamma_2 h + \gamma_1 z)} H_0^{(2)}(\lambda\rho)\lambda d\lambda \tag{13c}$$

$$\pi_{1z}(\rho,\phi,z) = -j \frac{I\ell}{4\pi\omega\varepsilon_2} \frac{k_2^2}{k_1^2} \cos\phi \frac{\partial}{\partial\rho} \left[\int_{-\infty}^{\infty} \frac{\gamma_2 - \gamma_1}{\gamma_2 k_1^2 + \gamma_1 k_2^2} e^{(\gamma_1 z - \gamma_2 h)} H_0^{(2)}(\lambda\rho)\lambda d\lambda \right] \tag{13d}$$

Thus, for $z > 0$,

$$E_\rho(\rho,\phi,z) = -j \frac{I\ell}{4\pi\omega\varepsilon_2} \cos\phi \left[\frac{\partial^2}{\partial\rho^2} \left(\frac{e^{-jk_2R_2}}{R_2} - \frac{e^{-jk_2R_1}}{R_1} + k_2^2 V_{22} \right) + \right.$$

$$+ k_2^2\left(\frac{e^{-jk_2R_2}}{R_2} - \frac{e^{-jk_2R_1}}{R_1} + U_{22}\right)\Bigg] \tag{14a}$$

$$E_\phi(\rho,\phi,z) = +j\frac{I\ell}{4\pi\omega\varepsilon_2}\sin\phi\left[\frac{1}{\rho}\frac{\partial}{\partial\rho}\left(\frac{e^{-jk_2R_2}}{R_2} - \frac{e^{-jk_2R_1}}{R_1} + k_2^2V_{22}\right)\right.$$

$$\left. + k_2^2\left(\frac{e^{-jk_2R_2}}{R_2} - \frac{e^{-jk_2R_1}}{R_1} + U_{22}\right)\right] \tag{14b}$$

$$E_z(\rho,\phi,z) = -j\frac{I\ell}{4\pi\omega\varepsilon_2}\cos\phi\frac{\partial^2}{\partial\rho\partial z}\left[\frac{e^{-jk_2R_2}}{R_2} + \frac{e^{-jk_2R_1}}{R_1} - k_1^2V_{22}\right] \tag{14c}$$

where V_{22} was given in (9) and U_{22} is defined as

$$U_{22} = \int_{-\infty}^{\infty}\frac{e^{-\gamma_2(z+h)}}{\gamma_1+\gamma_2}H_0^{(2)}(\lambda\rho)\lambda d\lambda = 2\int_0^{\infty}\frac{e^{-\gamma_2(z+h)}}{\gamma_1+\gamma_2}J_0(\lambda\rho)\lambda d\lambda \tag{15}$$

c) Difficulties encountered in numerical evaluation of the integrals:

Clearly, exact and closed form evaluation of these integrals V_{22}, U_{22} cannot be expected. When the point of observation is far from the sources, various asymptotic expressions, each being valid in different regions, may be used [7,8]. In the near field zone, however, numerical evaluation probably is the only viable way of obtaining numerical results. Three difficulties may be expected: rapid change of the values of the integrands near the branch points; oscillatory behaviour of the integrands due to the presence of the Hankel or Bessel functions; and the infinite range of integration [11,12]. By deforming the contour of integration, the troublesome regions near the branch points may be avoided. When the elevation of the

source points and/or the point of observation is moderate or high, enough damping factor is provided by the exponential functions to conceal the contribution from the oscillating factor for large values of λ. On the other hand, when z and h are both small, the effect of the exponential functions is negligible, the influence of the oscillating factor is accentuated, and the integrals are slow to converge.

3. Approximate Expressions

As mentioned in the last section when z+h is small the integrands decrease slowly as $|\lambda|$ increases. To illustrate this point, the integrand of V_{22} is examined for large values of $|\lambda|$. When $|\lambda|$ is large, $\gamma_i \approx |\lambda|$ and

$$\frac{2\lambda}{k_1^2\gamma_2+k_2^2\gamma_1} e^{-\gamma_2(h+z)} J_0(\lambda\rho) \approx \frac{|\lambda|}{\lambda} \frac{2}{k_1^2+k_2^2} e^{-|\lambda|(h+z)} \left[\sqrt{\frac{2}{\pi\rho\lambda}} \cos(\rho\lambda-\tfrac{\pi}{4}) + e^{|I_m\lambda|} O(\tfrac{1}{\lambda})\right]$$

where the asymptotic expression for the Bessel functions for large argument has been used. Clearly the integrand is an oscillatory function of $|\lambda|$ and decays as $|\lambda|^{-1/2}$ for large values of $|\lambda|$ if h+z is small. The rate of decay may be accelerated slightly by noting that for large values of $|\lambda|$,

$$\frac{\lambda}{k_1^2\gamma_2+k_2^2\gamma_1} e^{-\gamma_2(h+z)} \approx \frac{|\lambda|}{\lambda} \frac{1}{k_1^2+k_2^2} e^{-|\lambda|(h+z)}$$

then V_{22} may be written as

$$V_{22} = 2\int_0^\infty \left[\frac{\lambda}{k_1^2\gamma_2+k_2^2\gamma_1} e^{-\gamma_2(h+z)} - \frac{|\lambda|}{\lambda} \frac{1}{(k_1^2+k_2^2)} e^{-|\lambda|(h+z)}\right] J_0(\lambda\rho)d\lambda +$$

$$+ 2\int_0^\infty \frac{|\lambda|}{\lambda} \frac{1}{k_1^2+k_2^2} e^{-|\lambda|(h+z)} J_0(\lambda\rho)d\lambda \qquad (17)$$

The terms $|\lambda|/\lambda$ is introduced to retain the symmetry property of the integrand. Note the integrand of the first integral of (17) now decays as $|\lambda|^{-3/2}$ as $|\lambda| \to \infty$, and the second integral may be evaluated in closed-form, [13],

$$2\int_0^\infty \frac{|\lambda|}{\lambda} \frac{1}{k_1^2+k_2^2} e^{-|\lambda|(h+z)} J_0(\lambda\rho)d\lambda = \frac{2}{(k_1^2+k_2^2)R_1} \qquad (18)$$

where

$$R_1 = [\rho^2 + (z+h)^2]^{1/2}$$

U_{22} and derivatives of V_{22} are also rearranged in the same fashion:

$$\frac{\partial V_{22}}{\partial \rho} = 2\int_0^\infty \left[\frac{\lambda^2 e^{-\gamma_2(h+z)}}{k_1^2\gamma_2+k_2^2\gamma_1} - \frac{1}{k_1^2+k_2^2}\left(|\lambda| + \frac{k_2^2(h+z)}{2}\right) e^{-|\lambda|(h+z)}\right] J_0'(\lambda\rho)d\lambda$$

$$- \frac{2\rho}{k_1^2+k_2^2}\left(\frac{1}{R_1^3} + \frac{k_2^2(h+z)}{2R_1[(h+z)+R_1]}\right) \qquad (19)$$

$$\frac{\partial^2 V_{22}}{\partial \rho^2} = -2\int_0^\infty \left[\frac{\lambda^3 e^{-\gamma_2(h+z)}}{k_1^2\gamma_2 + k_2^2\gamma_1} - \frac{|\lambda|}{\lambda}\frac{\lambda^2 e^{-\lambda(h+z)}}{k_1^2 + k_2^2}\left(1+\frac{1}{2}\frac{k_2^2(h+z)}{|\lambda|} + \frac{k_1^2k_2^2}{(k_1^2+k_2^2)\lambda^2} + \frac{k_2^4(h+z)^2}{8\lambda^2}\right)\right] x$$

$$[J_0(\lambda\rho) + \frac{1}{\lambda\rho} J_0'(\lambda\rho)]d\lambda$$

$$- \frac{2}{k_1^2+k_2^2}\left[\left(-\frac{1}{R_1^3}+\frac{3(h+z)^2}{R_1^5}\right)+\frac{k_2^2}{2}\frac{(h+z)^3}{R_1^3}+\left(\frac{k_1^2k_2^2}{k_1^2+k_2^2}+\frac{k_2^4(h+z)^2}{8}\right)\frac{1}{R_1}\right]$$

$$+ \frac{2}{k_1^2+k_2^2}\left[\frac{1}{R_1^3}+\frac{1}{2}\frac{k_2^2(h+z)}{R_1[(h+z)+R_1]}+\left(\frac{k_1^2k_2^2}{(k_1^2+k_2^2)}+\frac{k_2^4(h+z)^2}{8}\right)\frac{1}{(h+z)R_1}\right] \qquad (20)$$

$$\frac{\partial^2 V_{22}}{\partial\rho\partial z} = -2\int_0^\infty \left\{\frac{\gamma_2\lambda^2}{k_1^2\gamma_2+k_2^2\gamma_1}e^{-\gamma_2(h+z)}\right.$$

$$\left. - \frac{e^{-|\lambda|(h+z)}}{(k_1^2+k_2^2)}\left[\lambda^2+\frac{1}{2}k_2^2(h+z)|\lambda|+\left(\frac{k_1^2k_2^2}{k_1^2+k_2^2}-\frac{1}{2}k_2^2+\frac{1}{8}k_2^4(h+z)^2\right)\right]\right\} J_0'(\lambda\rho)d\lambda$$

$$- \frac{2\rho}{k_1^2+k_2^2}\left[\frac{3(h+z)}{R_1^5}+\frac{1}{2}\frac{k_2^2(h+z)}{R_1^3}+\left(\frac{k_1^2k_2^2}{k_1^2+k_2^2}-\frac{1}{2}k_2^2+\frac{k_2^4(h+z)^2}{8}\right)\frac{1}{R_1[(h+z)+R_1]}\right] \qquad (21)$$

$$\frac{\partial^2 V_{22}}{\partial z^2} = 2\int_0^\infty \left[\frac{\lambda\gamma_2^2}{k_1^2\gamma_2+k_2^2\gamma_1}e^{-\gamma_2(h+z)}\right.$$

$$\left. - \frac{|\lambda|}{\lambda}\frac{e^{-|\lambda|(h+z)}}{k_1^2+k_2^2}\left(\lambda^2+\frac{|\lambda|k_2^2(h+z)}{2}-\frac{k_2^4}{k_1^2+k_2^2}+\frac{k_2^4(h+z)^2}{8}\right)\right] J_0(\lambda\rho)d\lambda$$

$$+ \frac{2}{k_1^2+k_2^2}\left\{\left[\frac{-1}{R_1^3}+\frac{3(h+z)^2}{R_1^5}\right]+\frac{1}{2}\frac{k_2^2(h+z)^2}{R_1^3}+\right.$$

$$\left[\frac{-k_2^4}{k_1^2+k_2^2} + \frac{k_2^4(h+z)^2}{8}\right]\frac{1}{R_1}\Bigg\} \tag{22}$$

$$U_{22} = 2\int_0^\infty \left[\frac{\lambda}{\gamma_1+\gamma_2} e^{-\gamma_2(h+z)} - \frac{1}{2}\frac{|\lambda|}{\lambda} e^{-|\lambda|(h+z)}\right] J_0(\lambda\rho)d\lambda + \frac{1}{R_1} \tag{23}$$

When these modifications were implemented in the computer code, a saving of 5% in computer time was achieved. Greater additional savings are obtained by using Hankel functions in the integrands instead of the Bessel functions [1,6]. The saving is particularly noticeable when $z+h \leq 0.01\ \lambda$.

However in calculating the self-impedance terms of thin wire segments, with radius $a << \lambda$, located a few radii above the interface, the modifications mentioned above are not enough. A possible explanation is as follows: For wires having extremely small radii, the Bessel and Hankel functions behave like $(\lambda\rho)^{1/2}$ only for extremely large values of $|\lambda|$. Fortunately, in computing the self-impedance terms of small wires, the distance between the source point and the point of observation is also small, thus the effect of time retardation or phase delay may be neglected. Mathematically, this is equivalent to approximating V_{22}, U_{22} and the derivatives of V_{22} by the closed-form expressions given in (18)-(23) and ignoring the contributions from the integrals yet to be evaluated. When the approximated expressions for V_{22}, U_{22} and the derivatives of V_{22} are substituted in (14a) and (14b), the resulting expressions for $E_{2\rho}$ and $E_{2\phi}$ agree with those derived by Bannister [14,15].

In the computer code, the approximations discussed above are used to calculate the interactions between points separated by 5 wire radii or less. For points spaced by a distance greater than 5 radii, the full expressions of (18)-(23) are used, including the integrals.

4. Monopole with a Ground Wire

The first configuration studied consists of a monopole with a single ground wire above a flat, lossy earth. The monopole is a perfectly conducting wire of radius .0381 m (1.5 inches) and length 5.62 m (18.44 ft.). A #1 wire (radius 3.67×10^{-3} m, (.01205 ft.)) is used as the ground wire and is located two radii above the earth surface. As mentioned by Brown et al [1], the current induced on the ground wire depends on the wire size in a logarithmic fashion. Thus the radii of the ground wires are not critical in determining the radiation properties of the ground screen systems. The wire size chosen here is based primarily on mechanical strength and economical considerations. The monopole is 5.62 m (18.44 ft.) long and is divided into three segments in the numerical calculation. These segments are labeled as shown in the insert of Fig. 2a. The length of the ground wire is incremented in steps of 1.86 m (6.12 ft.). The longest ground wire is 27.99 m (91.84 ft.) long and has 15 segments, numbered 4 through 18. A voltage source operating at 10 MHz is assumed to drive the monopole-ground wire system. For each configuration, the current at the center of each segment was computed with vanishing currents at the tip of the monopole, i.e., segment 1, and at the end of the last segment of the ground wire. The computed current was then normalized so that the magnitude of the current at the driven segment (segment 3) is 1.0 Ampere. Fig. 2a - 2j display the normalized current as a function of the segment number. Straight lines are drawn between the computed points to accentuate the trend of the variation of the current along the wires. The case of a ground wire having one segment is not included, since the current was forced to zero at the end of this segment, no information may be gained by displaying the normalized current at the center of the segment. In the calculation of Fig. 2a - 2j, the conduc-

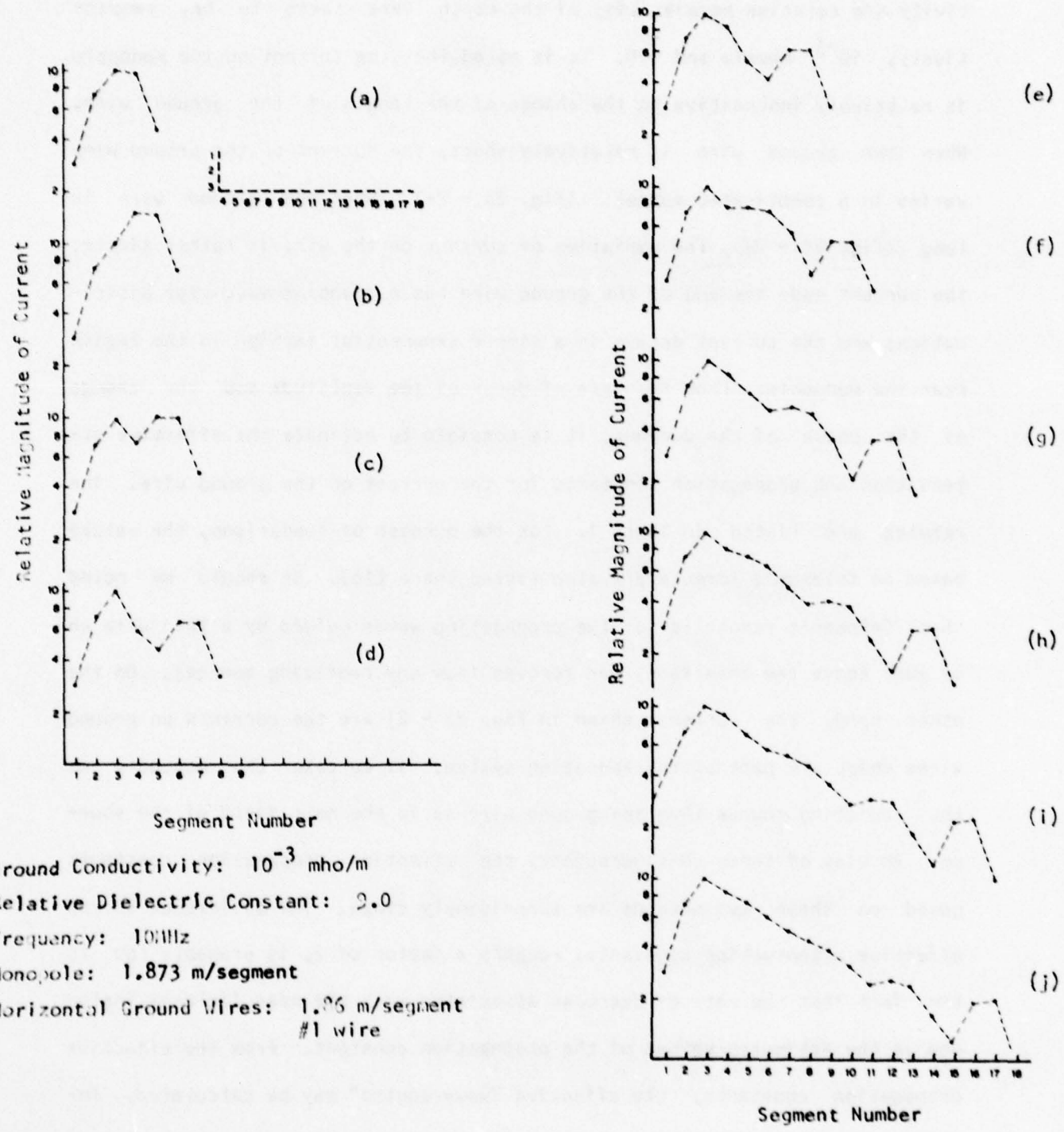

Ground Conductivity: 10^{-3} mho/m

Relative Dielectric Constant: 9.0

Frequency: 10MHz

Monopole: 1.873 m/segment

Horizontal Ground Wires: 1.86 m/segment
#1 wire

Figure 2. Normalized Current Distribution on a Short Monopole with a Single Ground Wire Over a Poor Ground ($\sigma = 10^{-3}$ mho/m $\varepsilon_R = 9.0$)

tivity and relative permittivity of the earth were taken to be, respectively, 10^{-3} mhos/m and 9.0. It is noted that the current on the monopole is relatively insensitive to the change of the length of the ground wire. When the ground wire is relatively short, the current on the ground wire varies in a complicated manner. (Fig. 2a - 2e). When the ground wire is long (Fig. 2f - 2j), the variation of current on the wire is rather simple: the current near the end of the ground wire has a standing-wave type distribution; and the current decays in a simple exponential fashion in the region near the monopole. From the rate of decay of the amplitude and the change of the phase of the current, it is possible to estimate the effective attenuation and propagation constants for the current on the ground wire. The results are listed in Table 1. For the purpose of comparison, the values based on Coleman's formula are also listed there [16]. It should be noted that Coleman's result is for the propagating waves guided by a thin wire on or just above the interface, far removed from any radiating sources. On the other hand, the currents shown in Fig. 2a - 2j are the currents on ground wires which are part of the radiating system. If we take the monopole as the radiating source then the ground wire is in the near field of the source. In view of these considerations, the effective propagation constants based on these two methods are surprisingly close. The difference in the effective attentuation constants, roughly a factor of 2, is probably due to the fact that the rate of decrease associated with the near field is included in the estimated values of the propagation constant. From the effective propagation constants, the effective "wavelengths" may be calculated. For most cases calculated, the current on the ground wire is smaller than that on the monopole. However, for the case of a ground wire of 5.58 m (18.3 ft.) in length (Fig. 2b) the current on the ground wire is larger than that

on the monopole by 50%. A plausible explanation is as follows: Since the far end of the ground wire is open-circuited, and the length of the ground wire is such that the impedance looking into the ground wire is very small, a major portion of the ground current would be expected to flow in the ground wire, rather than in the lossy earth. There is an alternative way of looking at this effect. For that particular length of ground wire, the total length of wire, (monopole plus ground wire) corresponds to the analog of a half wavelength resonant antenna system. However, part of the "antenna" wire is in one dielectric (air) while the other is in or near a second dielectric (earth). The wavelength in earth is shorter with the result that the maximum in the current standing wave pattern is on the ground wire part of the "antenna".

The current on the ground wire above a good ground ($\sigma = 10^{-2}$ mhos/m, and $\epsilon_r = 9.0$) has also been calculated. As shown in Fig. 3 the current distribution on the ground wire of 27.99 m (91.96 ft.) is almost identical to that on a ground wire of 26.16 m (85.83 ft.), except for the segments near the end. Also superimposed in the figure are the results for a 7.47 m. (24.52 ft.) ground wire. The fact that the current distributions in the region close to the monopole are so similar for the different lengths of the ground wire is mainly due to a large attenuation constant. The estimated effective attenuation and propagation constants of a good ground are also compared with that of Coleman's results in Table 1.

The vertical field patterns of the monopole with a ground wire of various lengths over a poor ground ($\sigma = 1 \times 10^{-3}$ mho/m and $\epsilon_r = 9.0$) as well as a better ground ($\sigma = 10^{-2}$ mho/m, and $\epsilon_r = 9.0$) are also calculated and are displayed in Fig. 4a, b and 5a,b. In these figures, E_θ in the forward direction ($\phi = 0^\circ$) is plotted as a function of θ. The time-average power

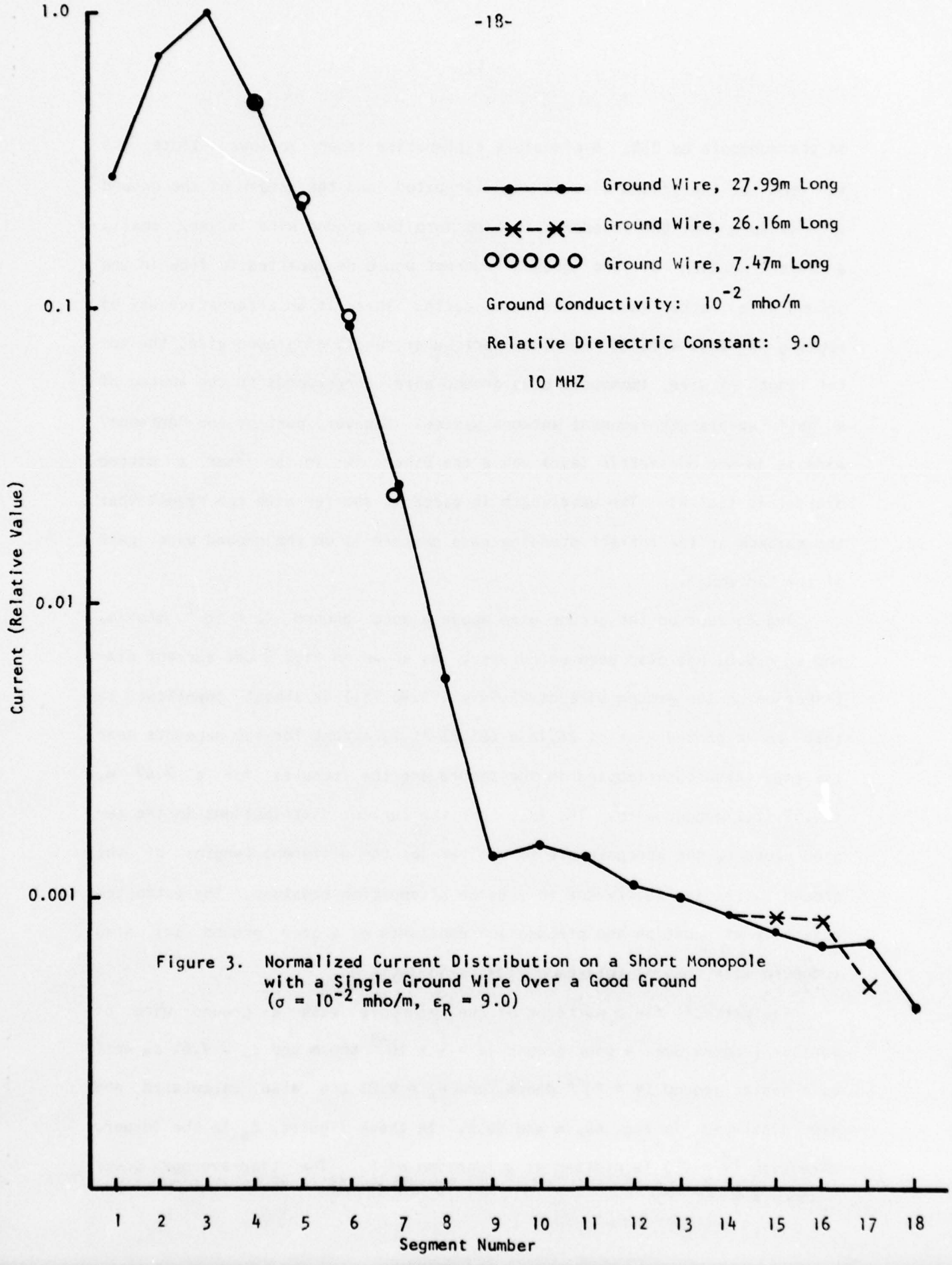

Figure 3. Normalized Current Distribution on a Short Monopole with a Single Ground Wire Over a Good Ground ($\sigma = 10^{-2}$ mho/m, $\varepsilon_R = 9.0$)

Table 1. Comparison of numerically estimated propagation and attenuation constants with that based on Coleman's formula, (10 MHz).

Ground Conductivity	(Mho/m.)	0.001	0.01
Ground Relative Permittivity		9.0	9.0
Results based on Coleman's formula	$\alpha + j\,\beta$ (m^{-1})	0.042 + j 0.469	.341 + j 0.579
	wavelength (m)	13.39	10.85
Values estimated from currents on the ground wire	$\alpha + j\,\beta$ (m^{-1})	0.09 + j 0.40	0.605 + j .675
	wavelength (m)	15.71	9.31

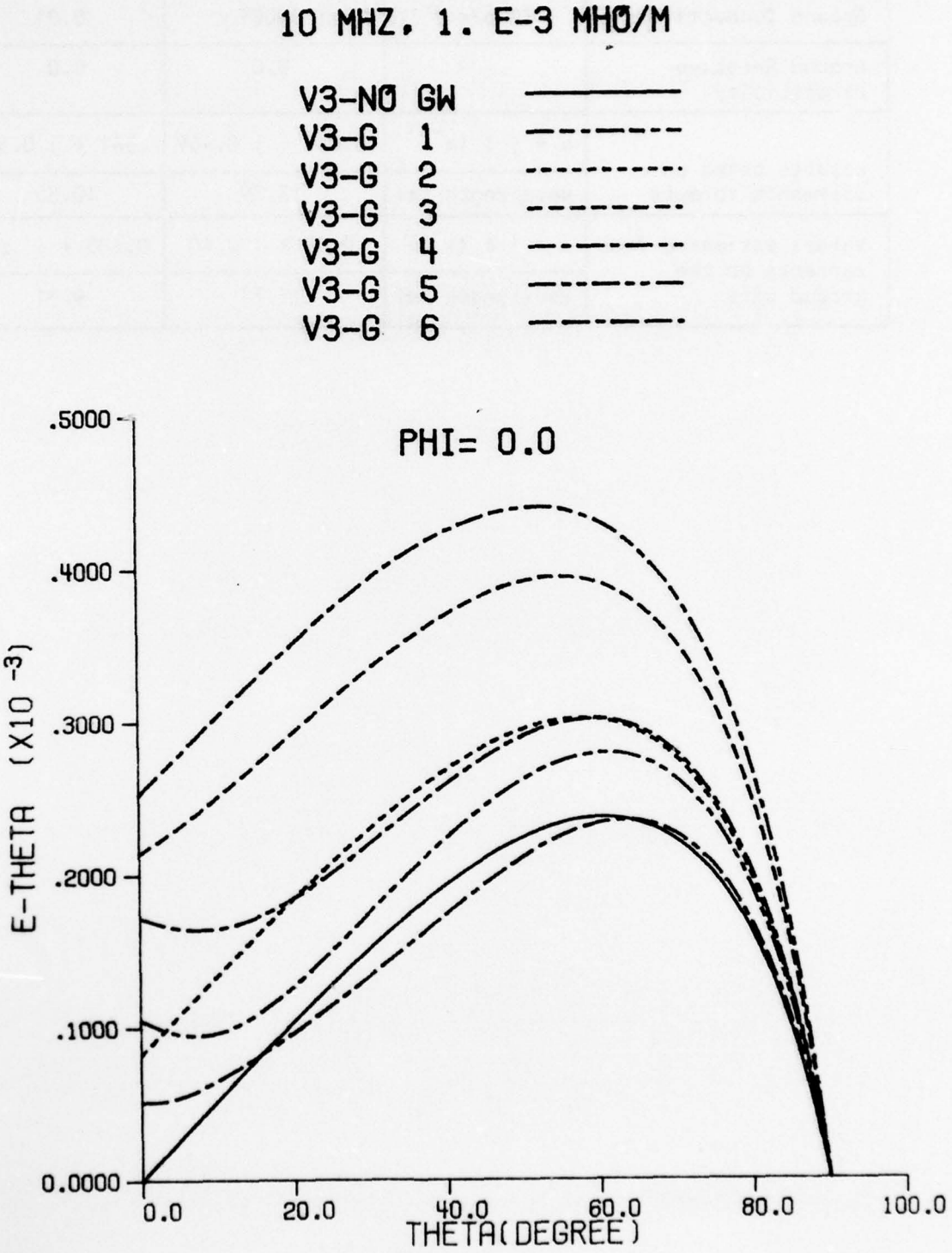

Figure 4a. Vertical Field Patterns of a Monopole with a Ground Wire Over a Poor Ground ($\sigma = 10^{-3}$ mho/m, $\varepsilon_R = 9.0$)

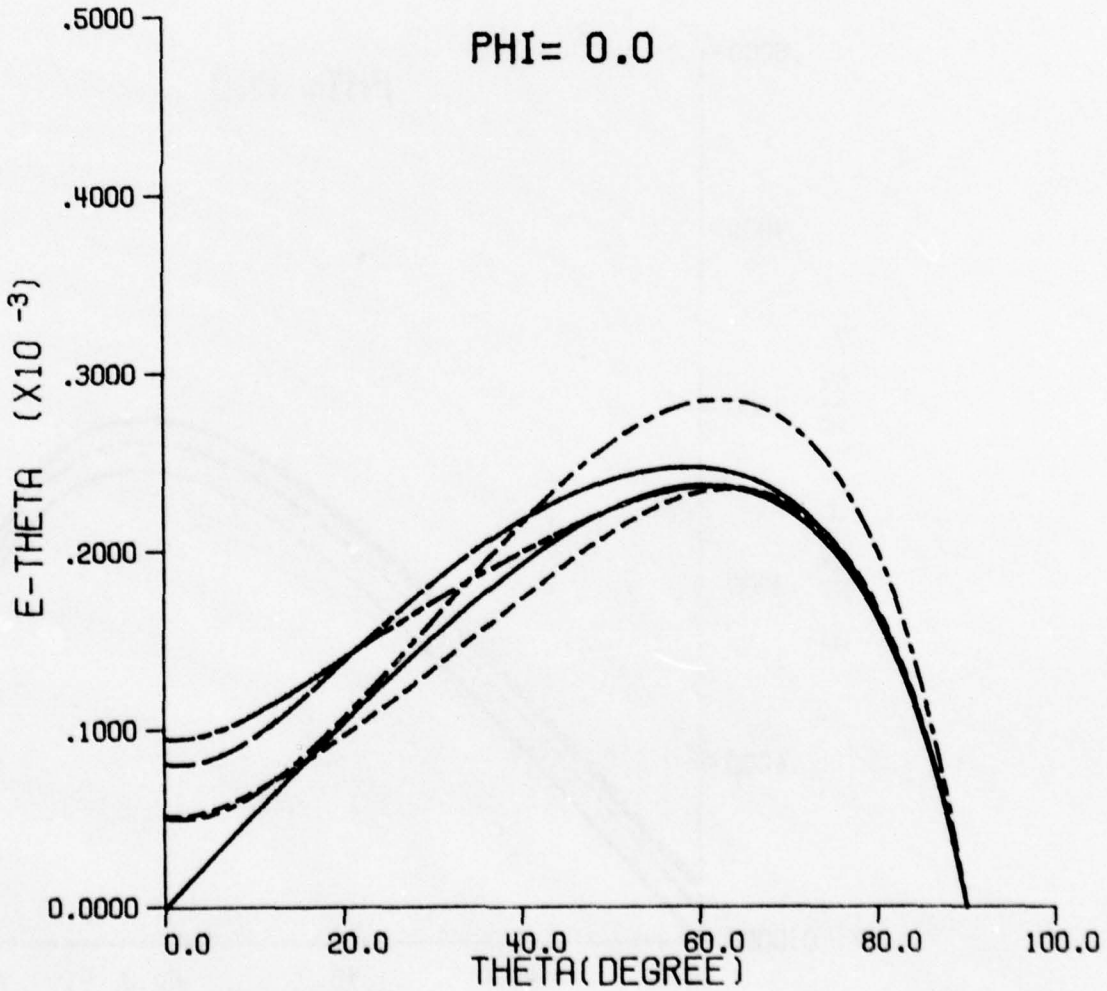

Figure 4b. Vertical Field Patterns of a Moropole with a Ground Wire Over a Poor Ground ($\sigma = 10^{-3}$ mho/m, $\epsilon_R = 9.0$)

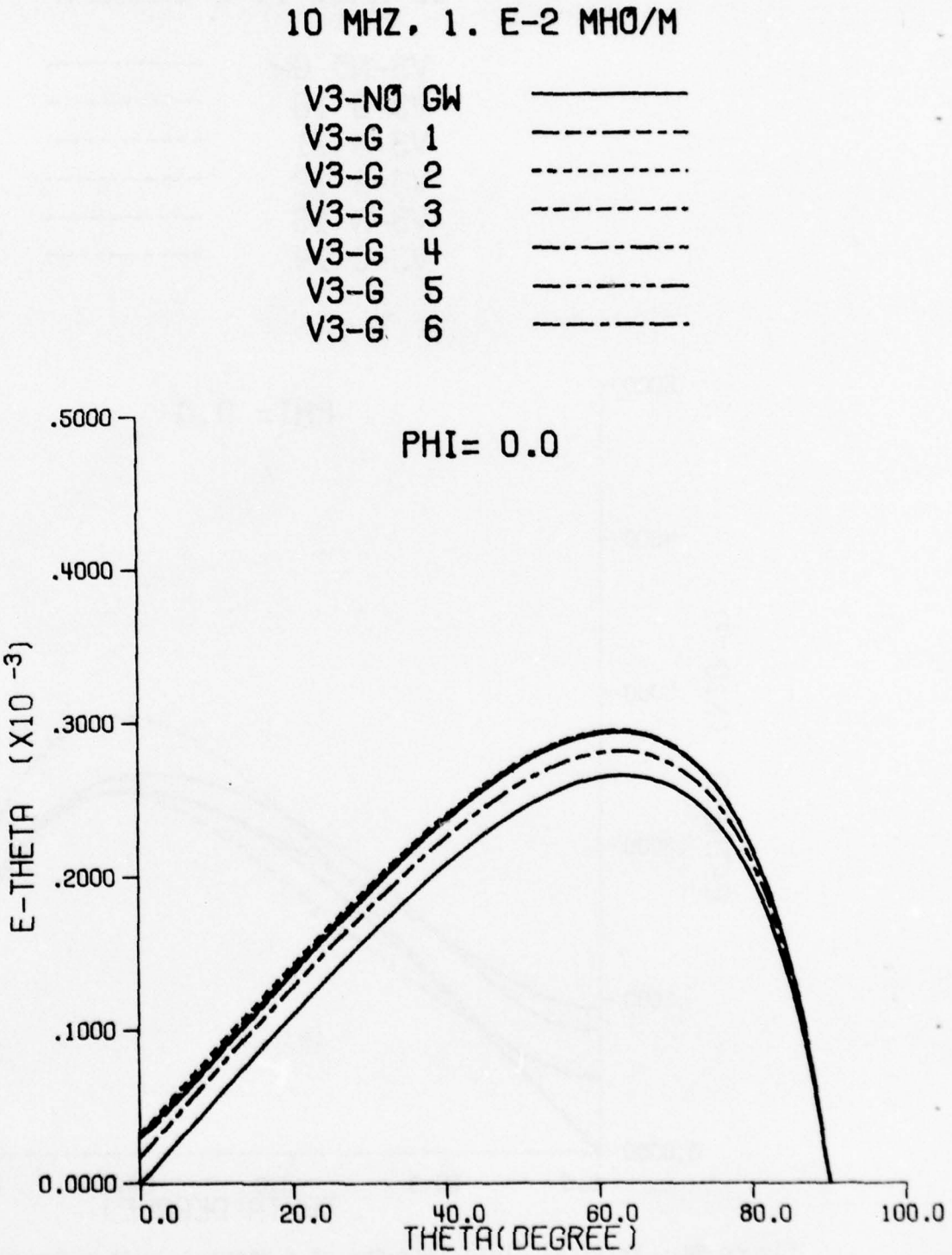

Figure 5a. Vertical Field Patterns of a Monopole with a Ground Wire Over a Good Ground ($\sigma = 10^{-2}$ mho/m, $\varepsilon_R = 9.0$)

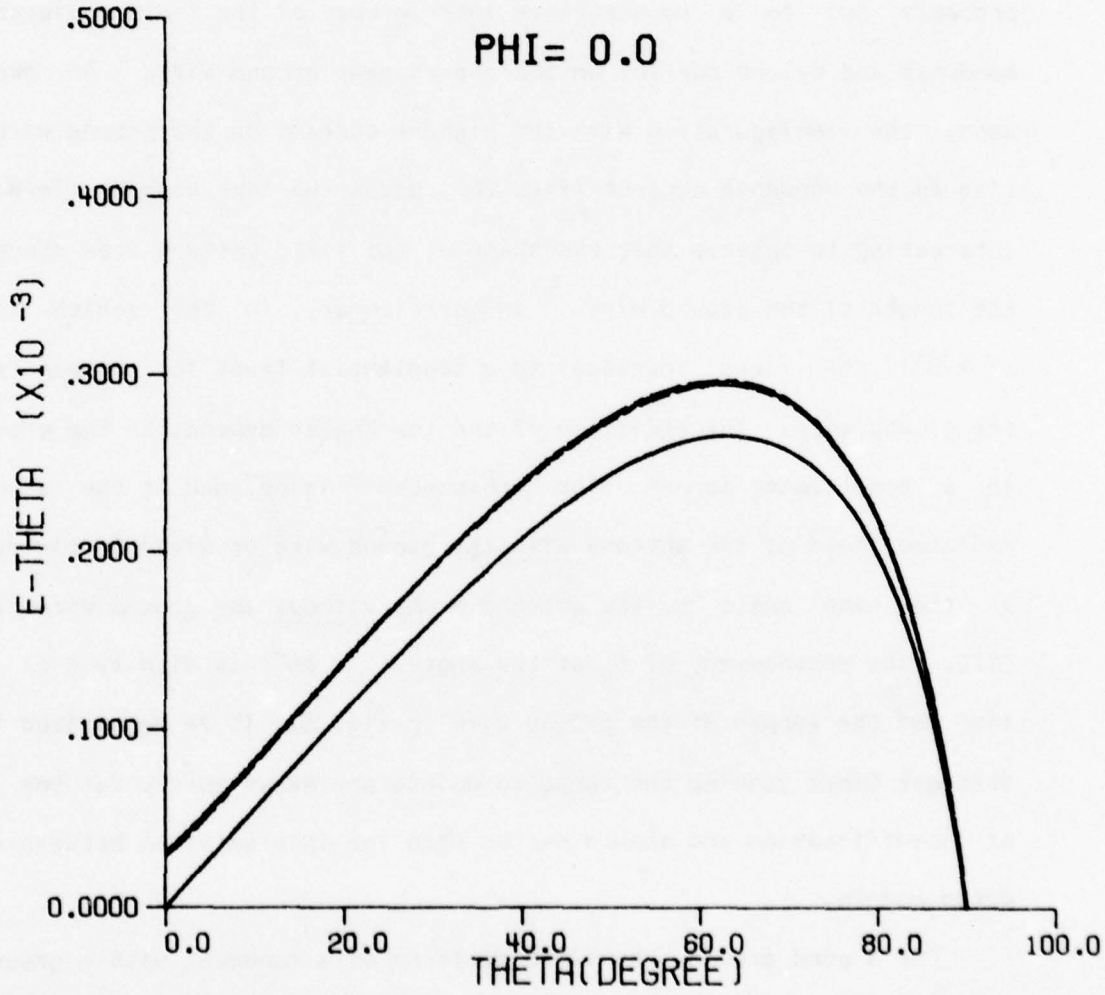

Figure 5b. Vertical Field Patterns of a Monopole with a Ground Wire Over a Good Ground ($\sigma = 10^{-2}$ mho/m, $\epsilon_R = 9.0$)

input to the monopole is fixed at 1 watt. The length of the ground wire is indicated in the legend. For example, V3-G 12 signifies that there are three segments on the monopole and 12 segments on the ground wire. The field pattern of the monopole without the ground wire is included in all figures to facilitate the comparison. When a poor ground is involved, the intensity of the radiated field varies considerably, reflecting the change in the input impedance of the radiating system as a function of the length of the ground wire. The configuration consisting of the monopole and a ground wire with one segment gives the greatest radiated field. This is probably due to a constructive interference of the field radiated by the monopole and by the current on the one-segment ground wire. On the other hand, the configuration with the highest current on the ground wire, relative to the monopole current (Fig. 2b), gives the next highest field. It is interesting to observe that the shape of the field pattern also changes with the length of the ground wire. In particular, in the zenith direction ($\theta = 0°$) the field increases to a substantial level for certain length of the ground wire. The radiation at the low angles depends on the ground wire in a complicated manner. The "enhancement" is defined as the ratio of the radiated field of the antenna with the ground wire or wires to the radiation at the same angle by the antenna alone without any ground wire or screen [17]. The enhancement of E_θ at low angle ($\theta = 86°$) is displayed as a function of the length of the ground wire in Fig. 6. It is emphasized that the straight lines joining the computed points are drawn purely for the purpose of identification and should not be used for interpolation between the computed points.

For a good ground, the field patterns of a monopole with a ground wire of two or more segments coincide with each other; only the patterns due to

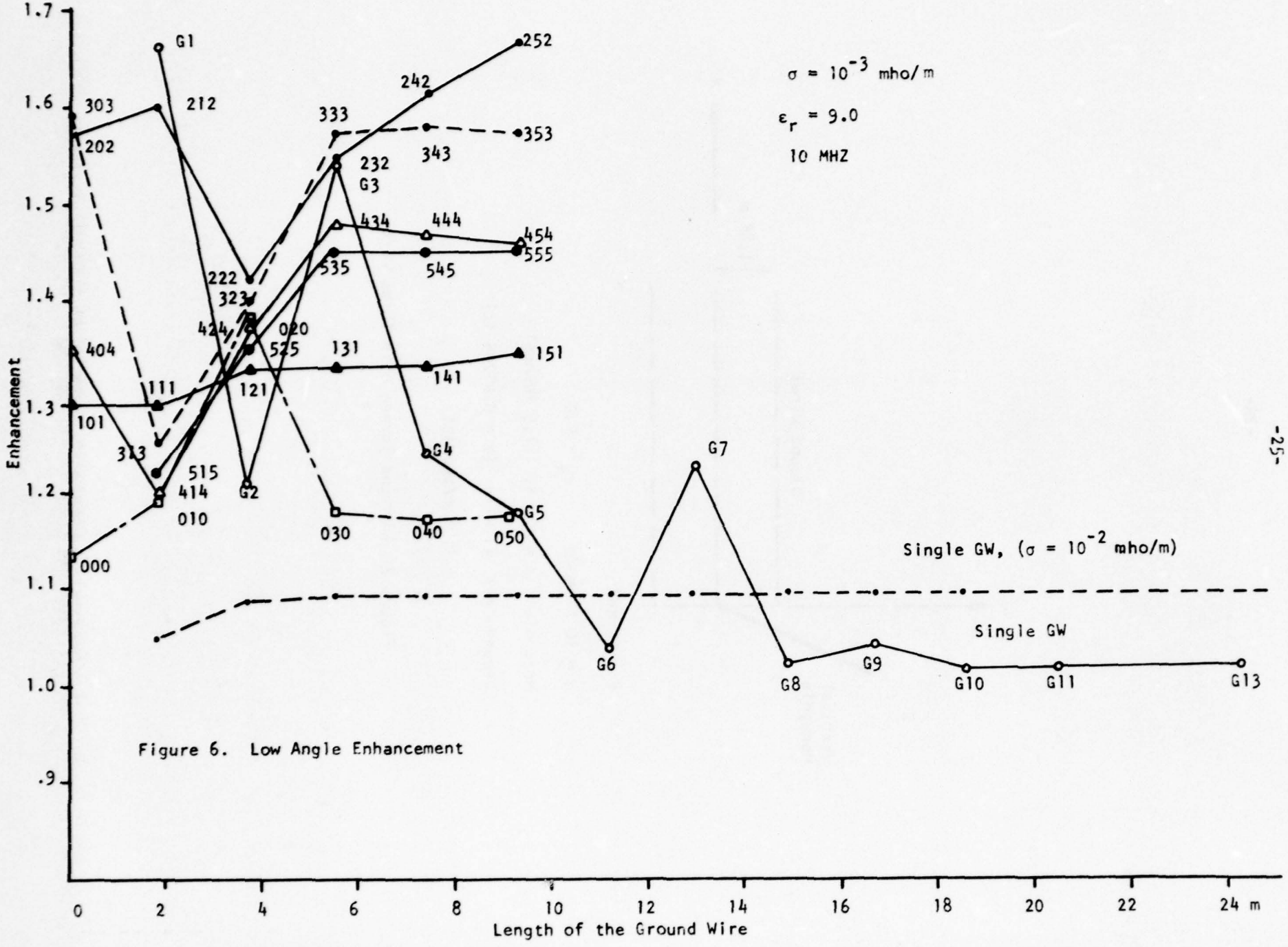

Figure 6. Low Angle Enhancement

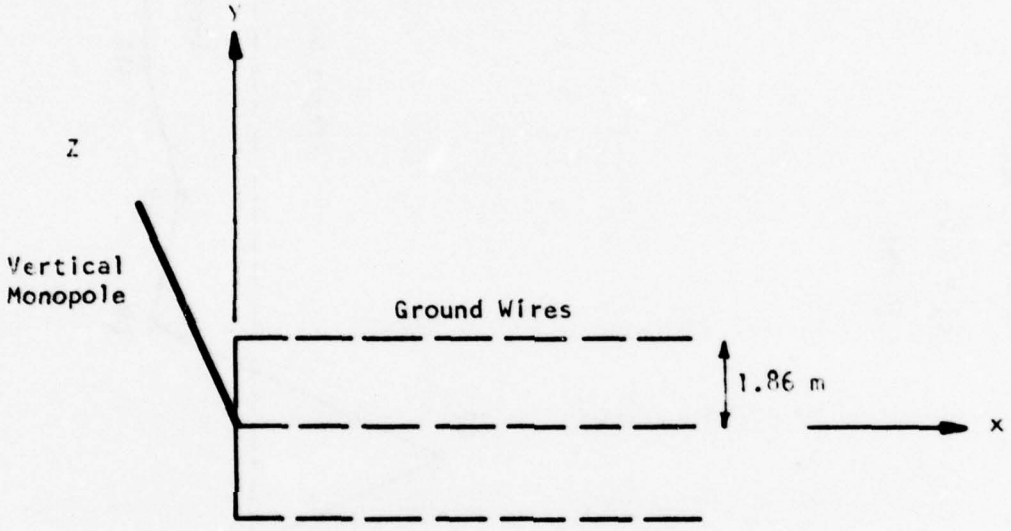

f = 10 MHZ

$\sigma = 10^{-3}$ mho/m $\quad \varepsilon_R = 9.0$

Monopole: a = .125 ft (1.5 inches)

Groundwire: #1 wire (a = 0.01205 ft)

1.86 m/segment

Figure 7. A Ground Screen with Three Wires

the monopole without a ground wire or with a ground wire of one segment are distinguishable from the rest as shown in Fig. 5a and 5b. The dependence of the low-angle enhancement on the length of the ground wire also varies in a simple fashion, as shown in Fig. 6.

5. Monopole with Ground Screens of Three Wires

Next we consider a ground screen with three ground wires forming a three-legged fork in the forward direction, as shown in Fig. 7. Our computation scheme permits each wire to have five or less segments in the x-direction. For each configuration, a three digit number is assigned to represent the number of segments in each leg. For example, 242 indicates that there are two segments in the two outer wires and four segments in the center wire. The segments along the y-axis are not included in the designation. Figs. 8-13 show the vertical field patterns in the forward direction ($\phi = 0°$) with ground screens of various shapes. The frequency and radii of wires are the same as used in Sec. 4 and a poor ground with a conductivity of 10^{-3} mho/m is assumed. In each set of the curves, the number of segments in the two outer wires is fixed while the length of the center wire is varied. Although the field patterns are roughly alike, including the pattern due to the three-segment monopole without any ground wire, the level of radiation varies considerably. The enhancement at the low angle is also calculated and displayed in Fig. 6. Of all cases computed, the ground screen with 252 arrangement is the most effective one in increasing the low-angle radiation. Since considerable enhancement can also be provided by 242 or 232 arrangements, it is conjectured that a ground screen of this shape is probably insensitive to the frequency variation. The vertical patterns due to the 252 ground screen are also obtained for $\phi = 30°$, $45°$, $90°$, $135°$ and $180°$ (Fig. 14).

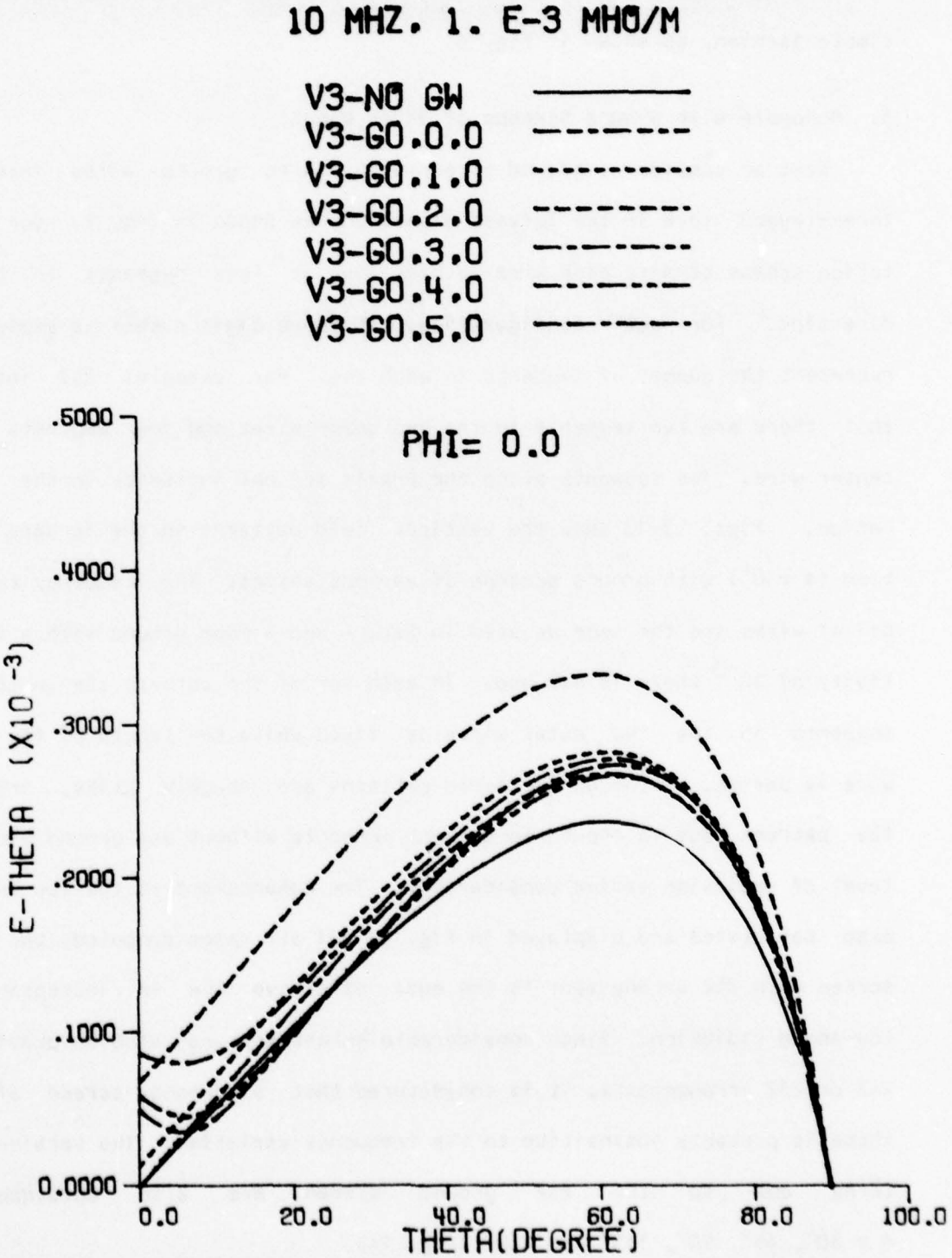

Figure 8. Vertical Field Patterns (ϕ=0°) of Ground Screens of ONO Configuration

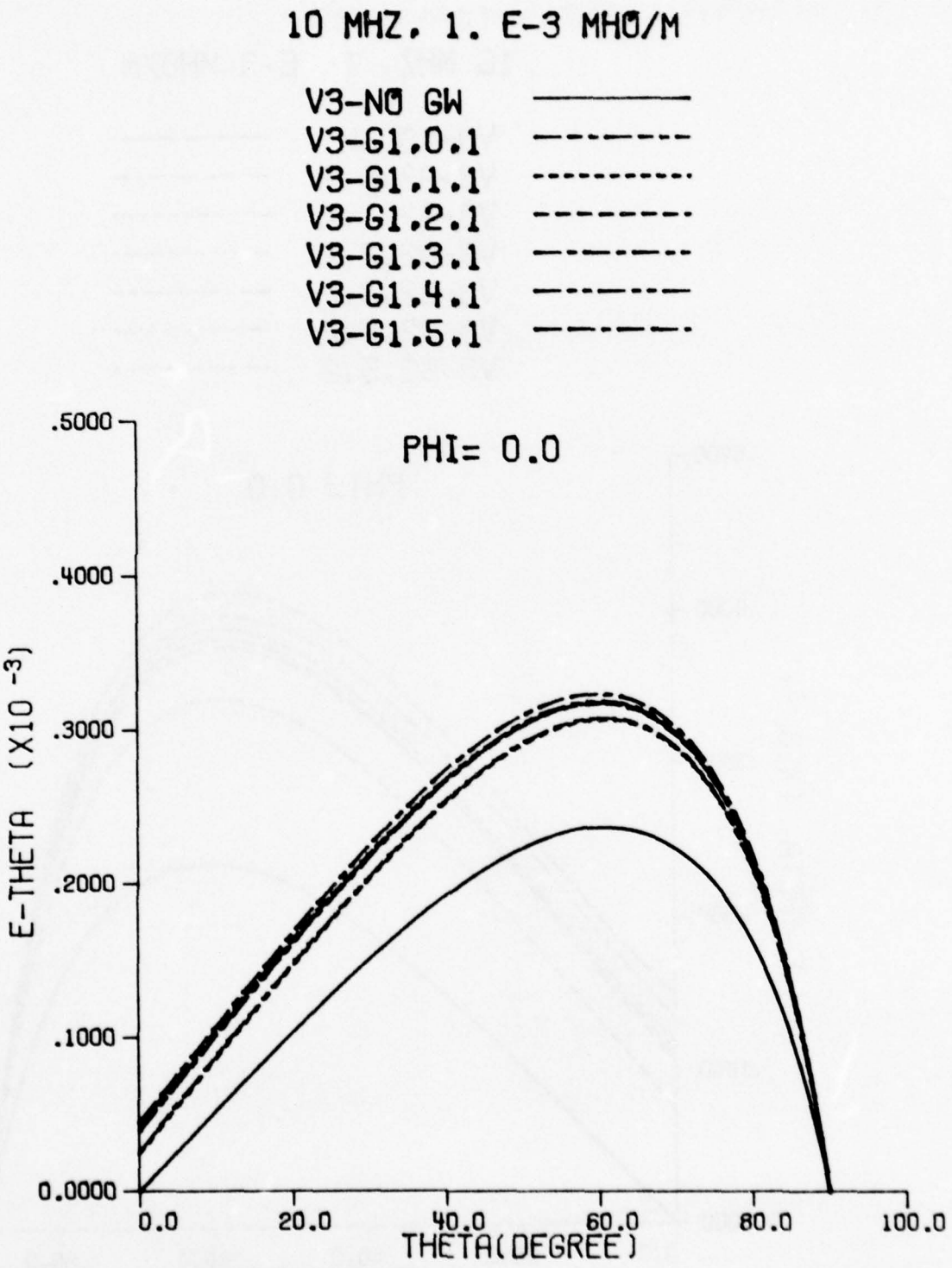

Figure 9. Vertical Field Patterns (ϕ=0°) of Ground Screens of IN1 Configuration

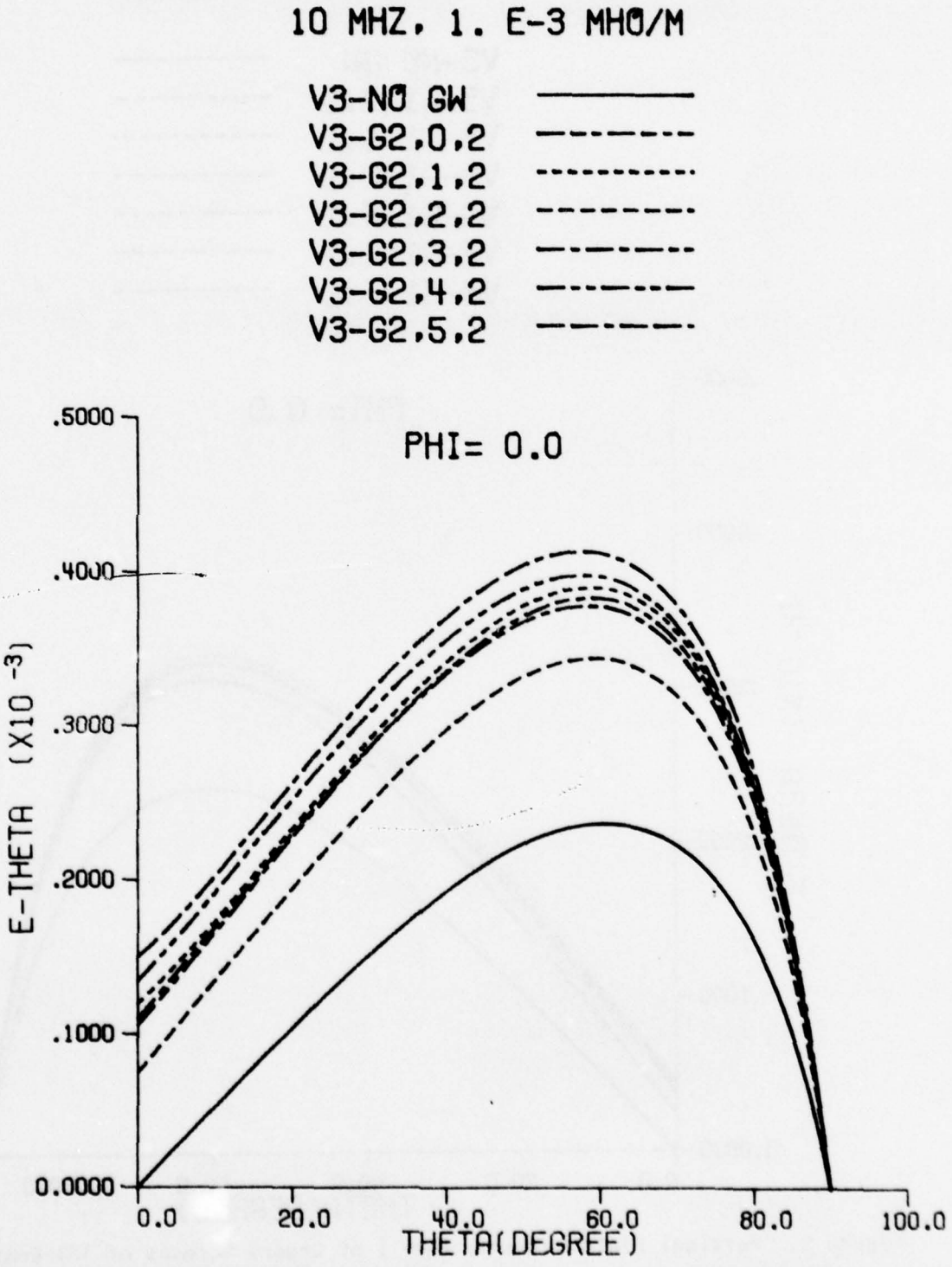

Figure 10. Vertical Field Patterns (ϕ=0°) of Ground Screens of 2N2 Configuration

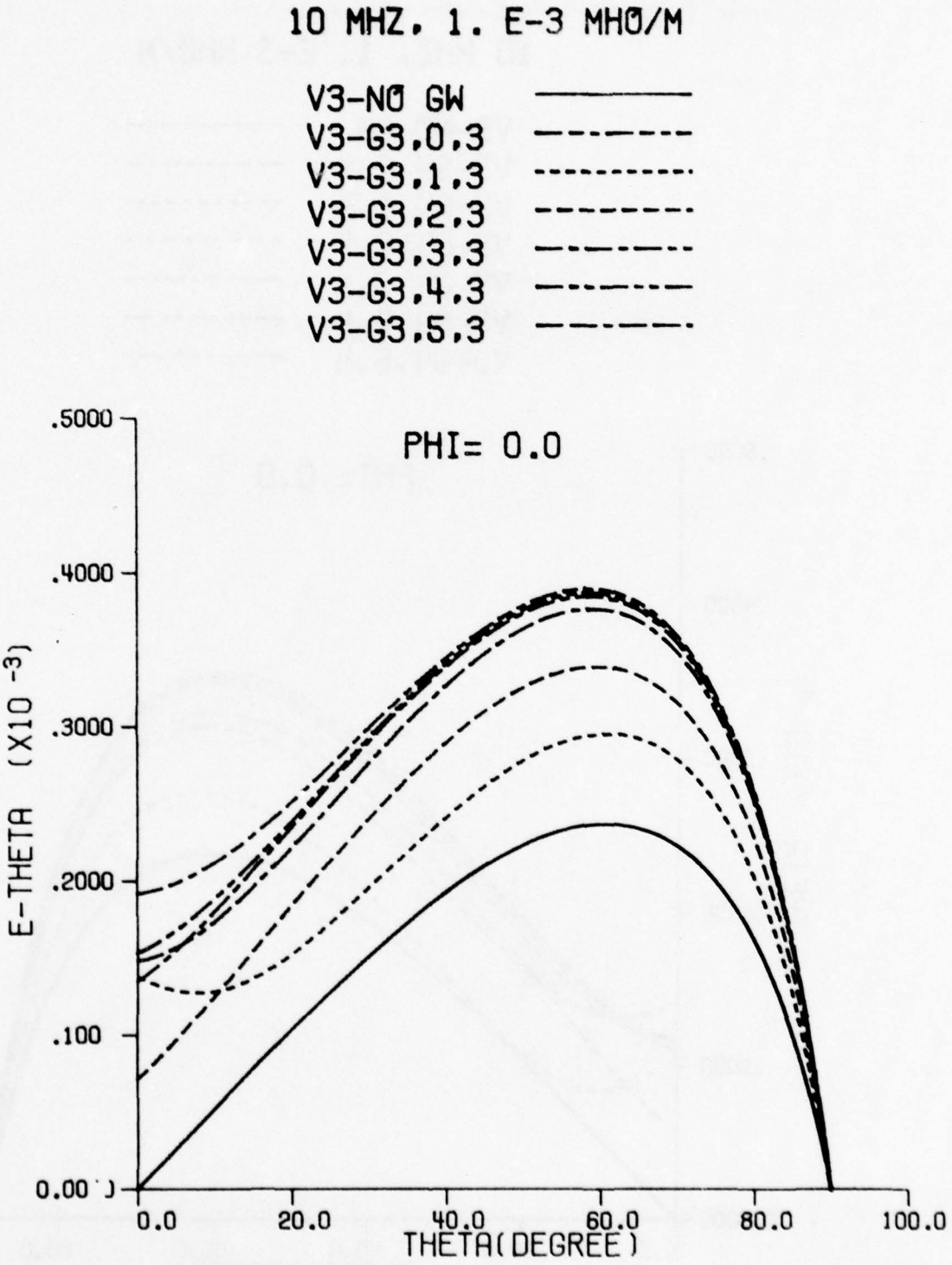

Figure 11. Vertical Field Patterns (ϕ=0°) of Ground Screens of 3N3 Configuration

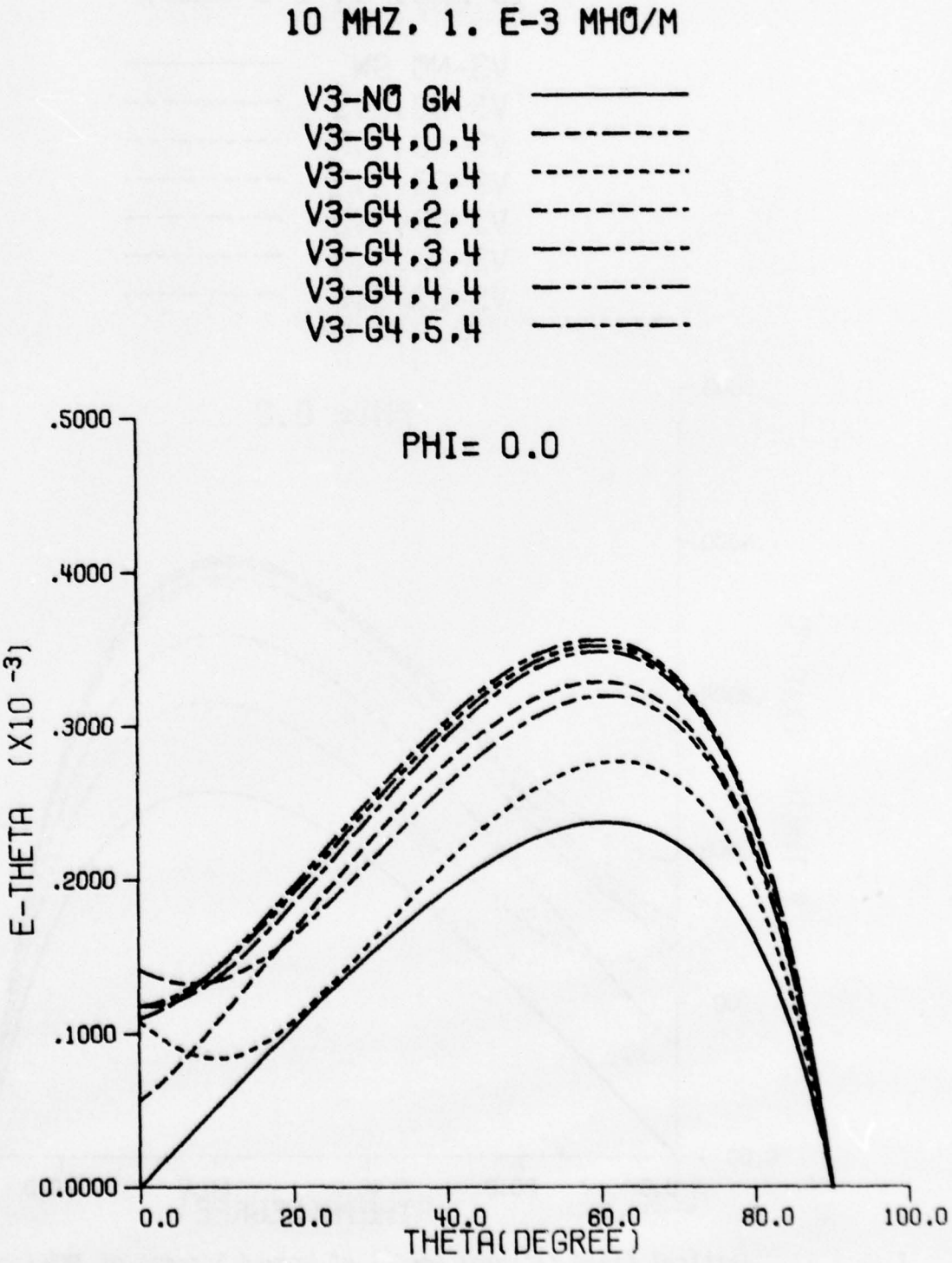

Figure 12. Vertical Field Patterns (ϕ=0°) of Ground Screens of 4N4 Configuration

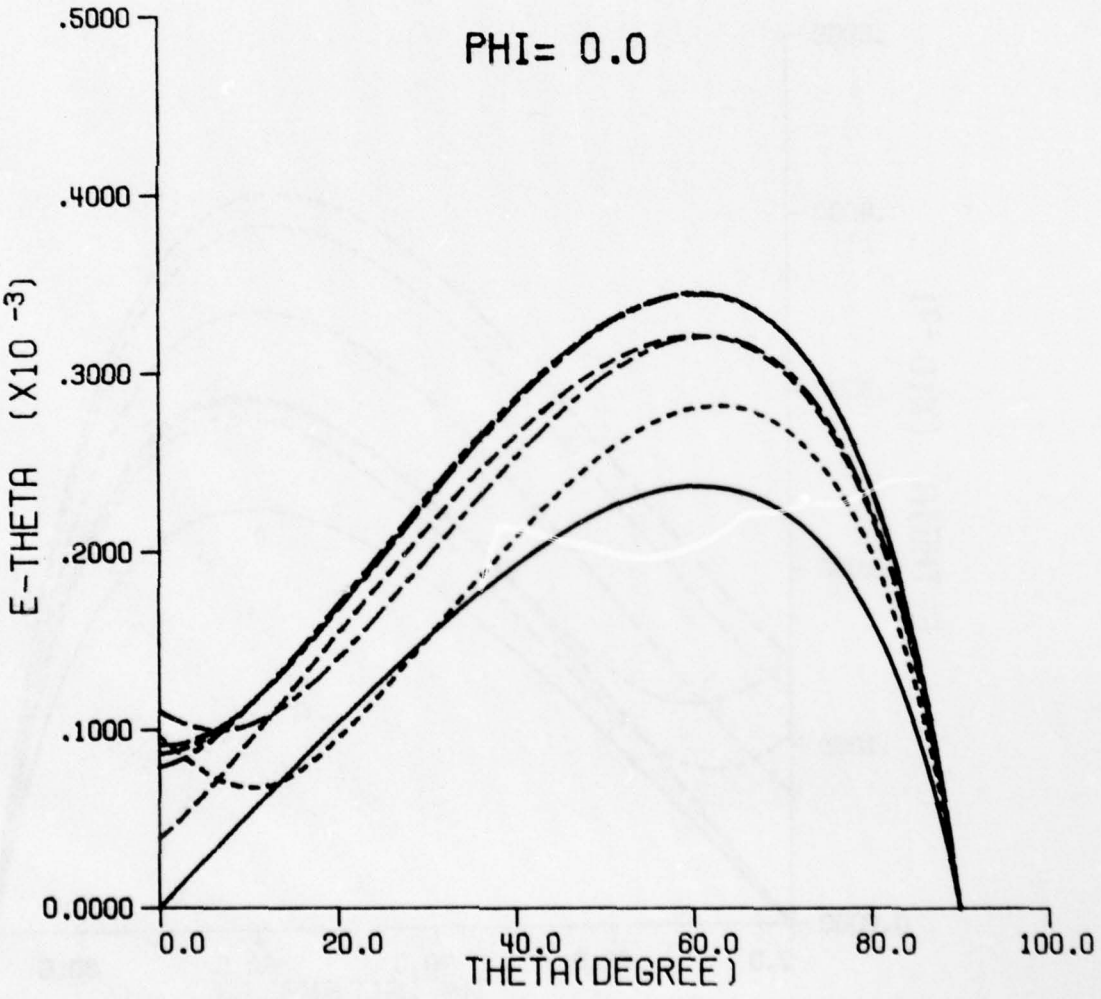

Figure 13. Vertical Field Patterns (ϕ=0°) of Ground Screens of 5N5 Configuration

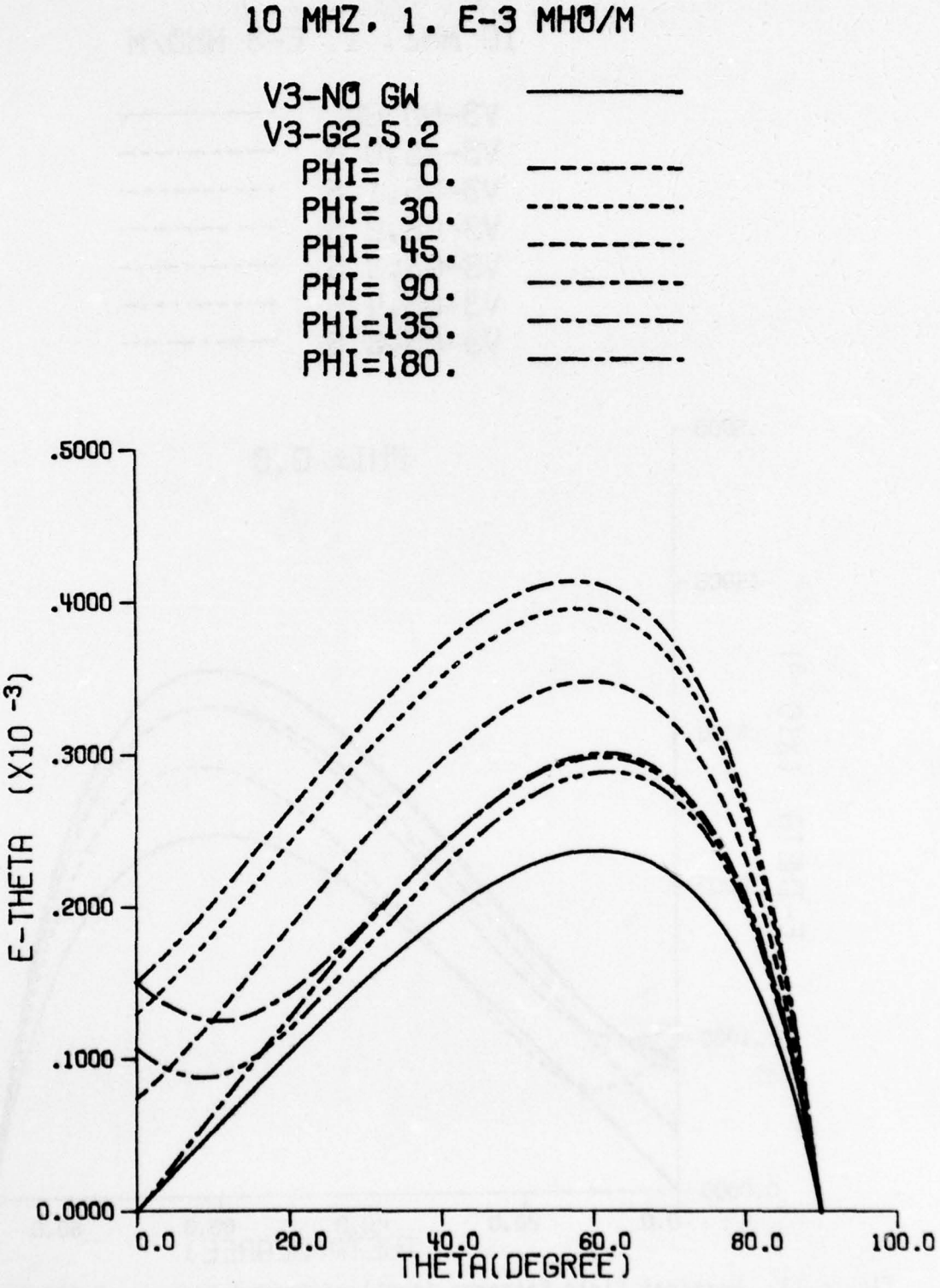

Figure 14. Vertical Field Patterns of Ground Screen 252 at Various Angles

6. Monopole with Ground Screens of Four Wires

Ground screens consisting of four ground wires forming a right angle cross as shown in Fig. 15a, 15b were also studied. The monopole is divided into six segments of equal lengths (.457 m., (1.5 ft.)). Each ground wire may have at most 13 segments. The four segments near the monopole have lengths of .457 m (1.50 ft.), 0.785 m (2.58 ft.), 1.35 m (4.42 ft.) and 2.32 m (7.59 ft.) respectively. The nine segments farther away from the monopole each have the same length, 3.05 m (10.0 ft.). Each ground screen is designated by a four-digit number representing the numbers of segments in the ground wires. A ground conductivity of 10^{-3} mho/m, a relative permittivity of 5.0 and a frequency of 2 MHz are used in the calculation. Again the vertical patterns are of the same general shape as shown in Fig. 16. It is interesting to note that the radiation field increases or decreases for all angles at the same time as the length of the ground screen is being changed. To demonstrate this point further, the enhancement at the low angle ($\theta = 87°$) and at ($\theta = 60°$), which is very close to the peak of the radiation patterns, are plotted as functions of ϕ for four different ground screens in Fig. 17. Note that for each ground screen, the enhancement at $\theta = 87°$ varies in the same manner as that at $\theta = 60°$. To examine the role played by the ground wires in the backward direction, the length of two wires in the backward directions are decreased while the length of two wires in the forward direction remains unchanged (Fig. 15b). The resulting low-angle enhancement is shown in Fig. 18a, 18b. An extreme case would be to remove the wires in the backward direction completely forming a right-angle Vee. The enhancement of the ground screens of 90° Vee shape with various length of wires is shown in Fig. 19a and 19b. These results are summarized in Fig. 20 where the low-angle enhancement in the forward and backward directions is

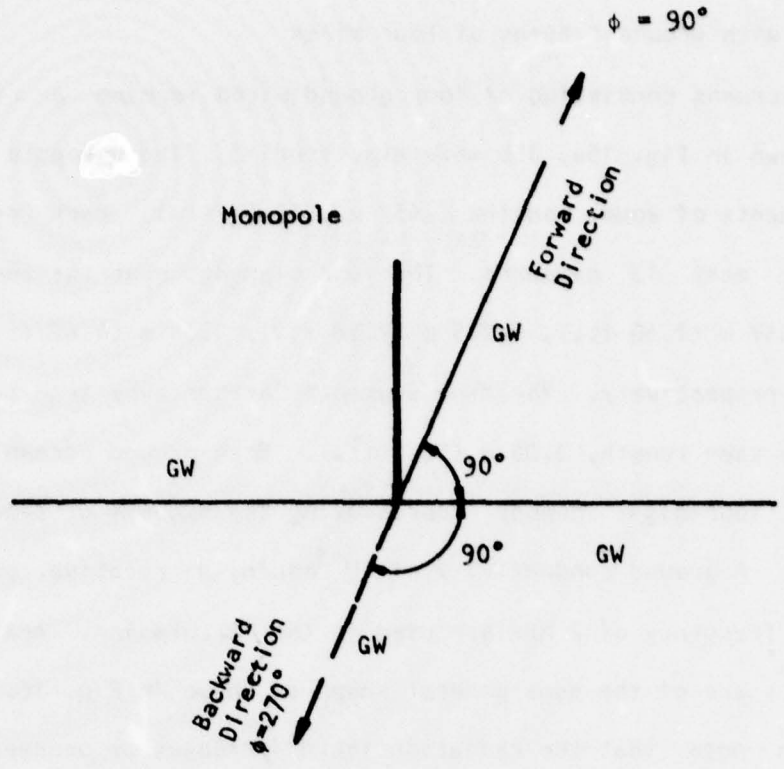

(a)

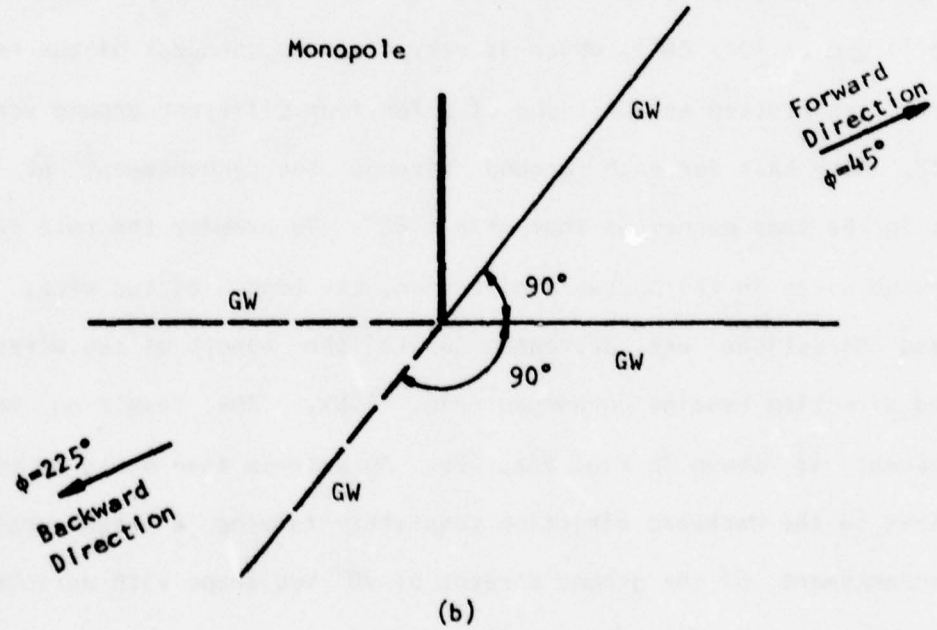

(b)

Figure 15. Ground Screens with Four Wires

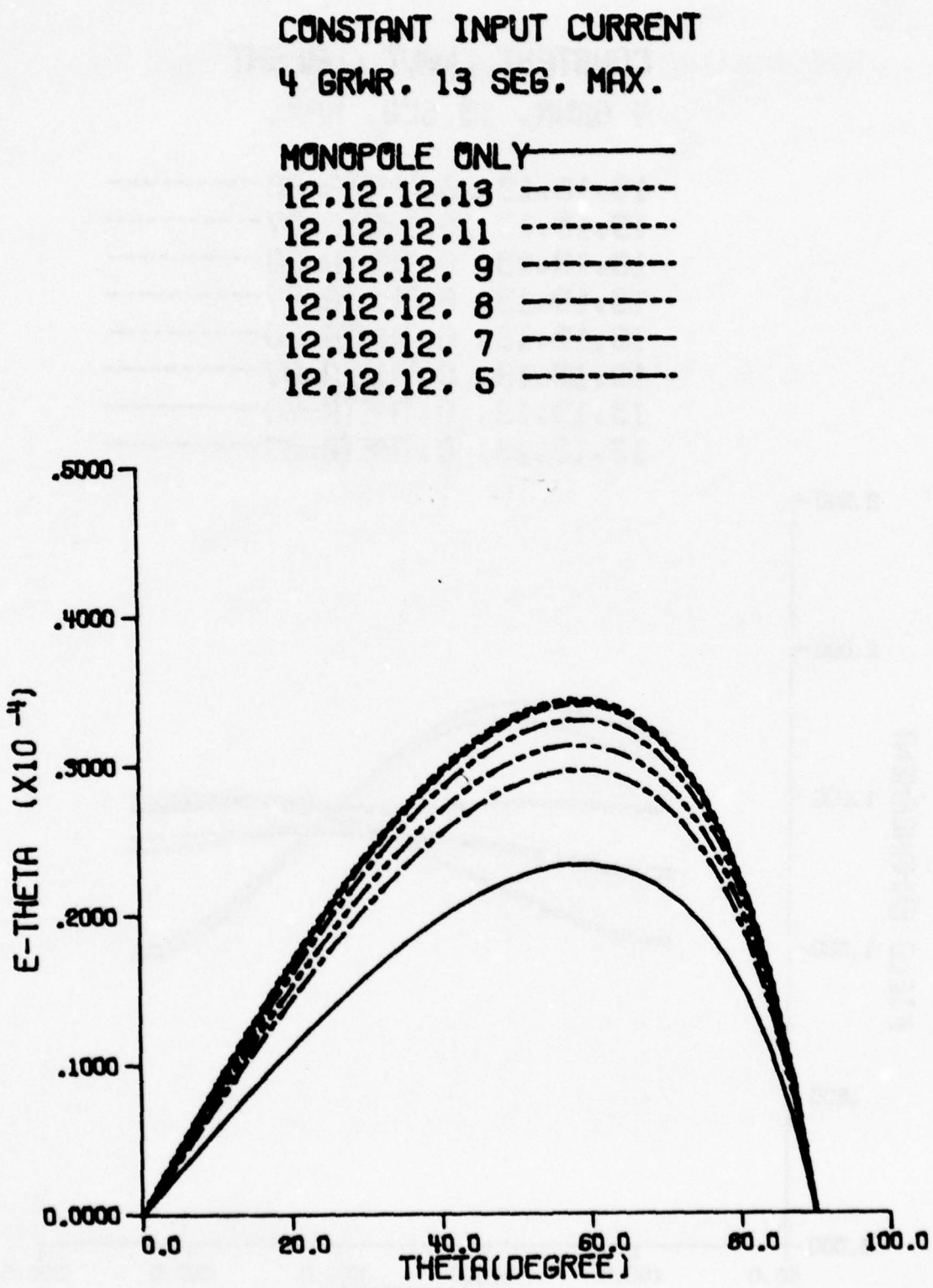

Figure 16. Vertical Field Patterns (ϕ=90°) of Ground Screens of Four Wires with (12, 12, 12, N) Configuration

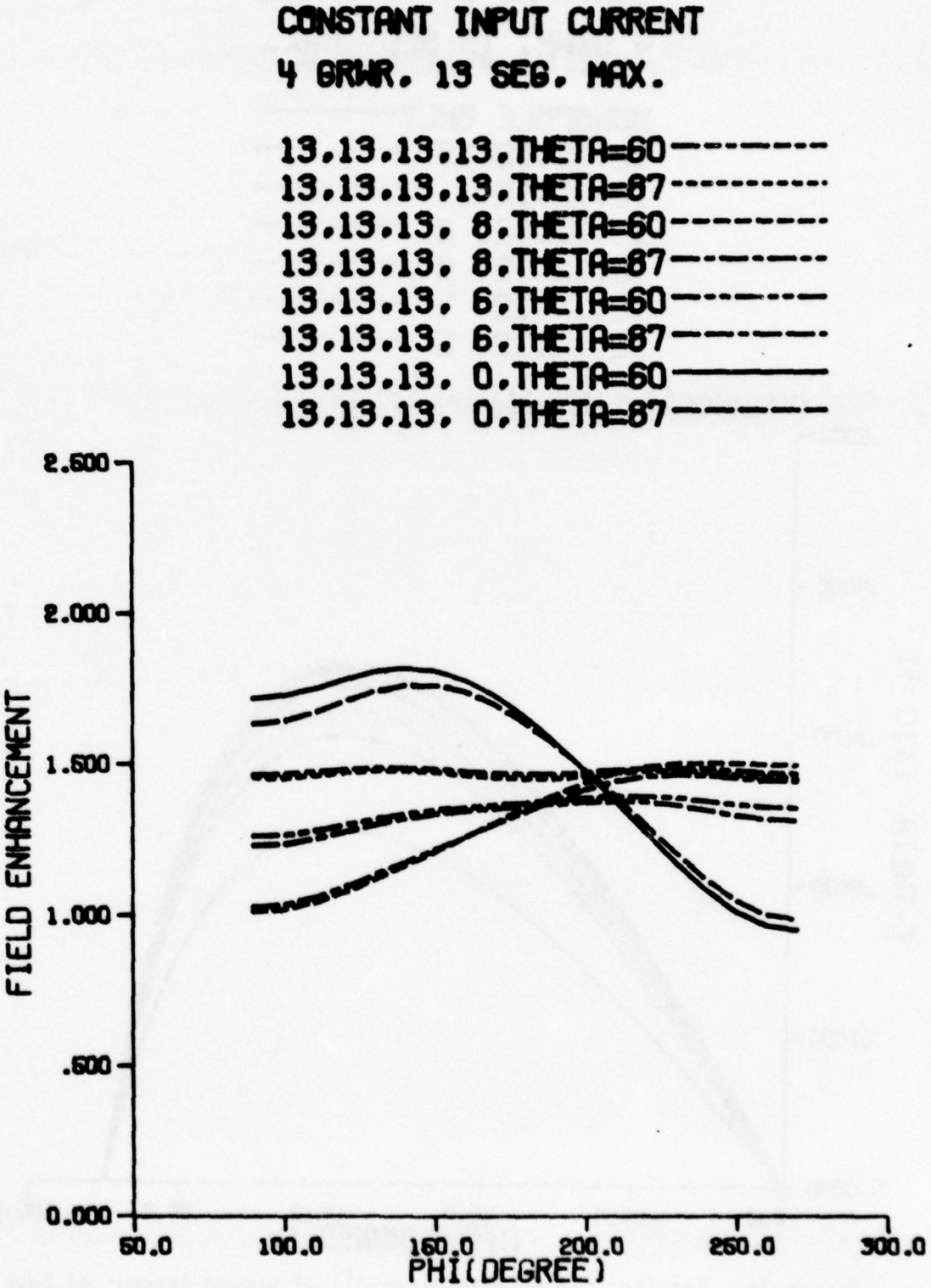

Figure 17. Field Enhancement at θ=60° and θ=87° for Four-Wire Ground Screens with (13, 13, 13, N) Configuration

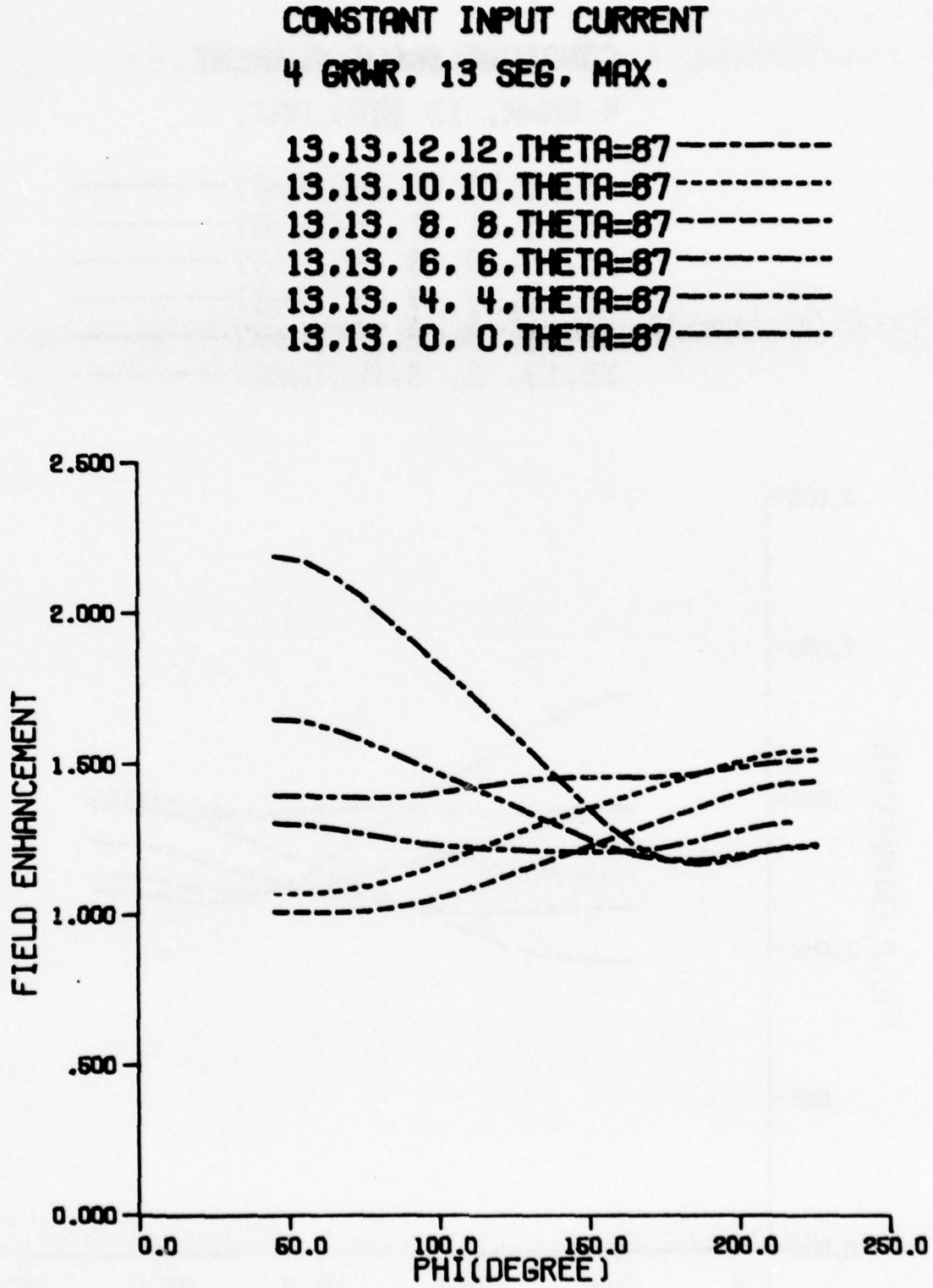

Figure 18a. Low Angle Field Enhancement (θ=87°) for Four-Wire Ground Screens of (13, 13, N, N) Configuration

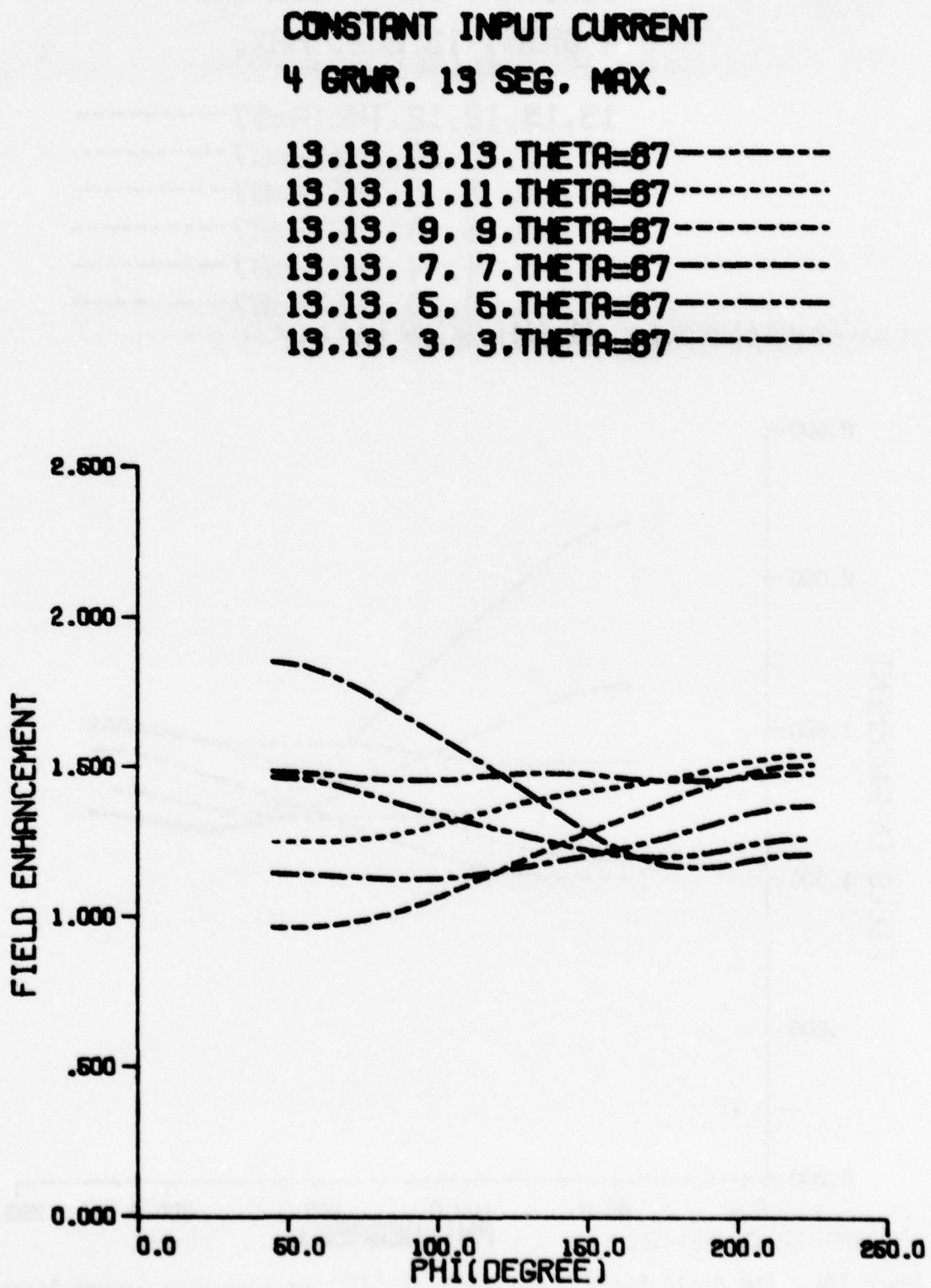

Figure 18b. Low Angle Field Enhancement (θ=87°) for Four-Wire Ground Screens of (13, 13, N, N) Configuration

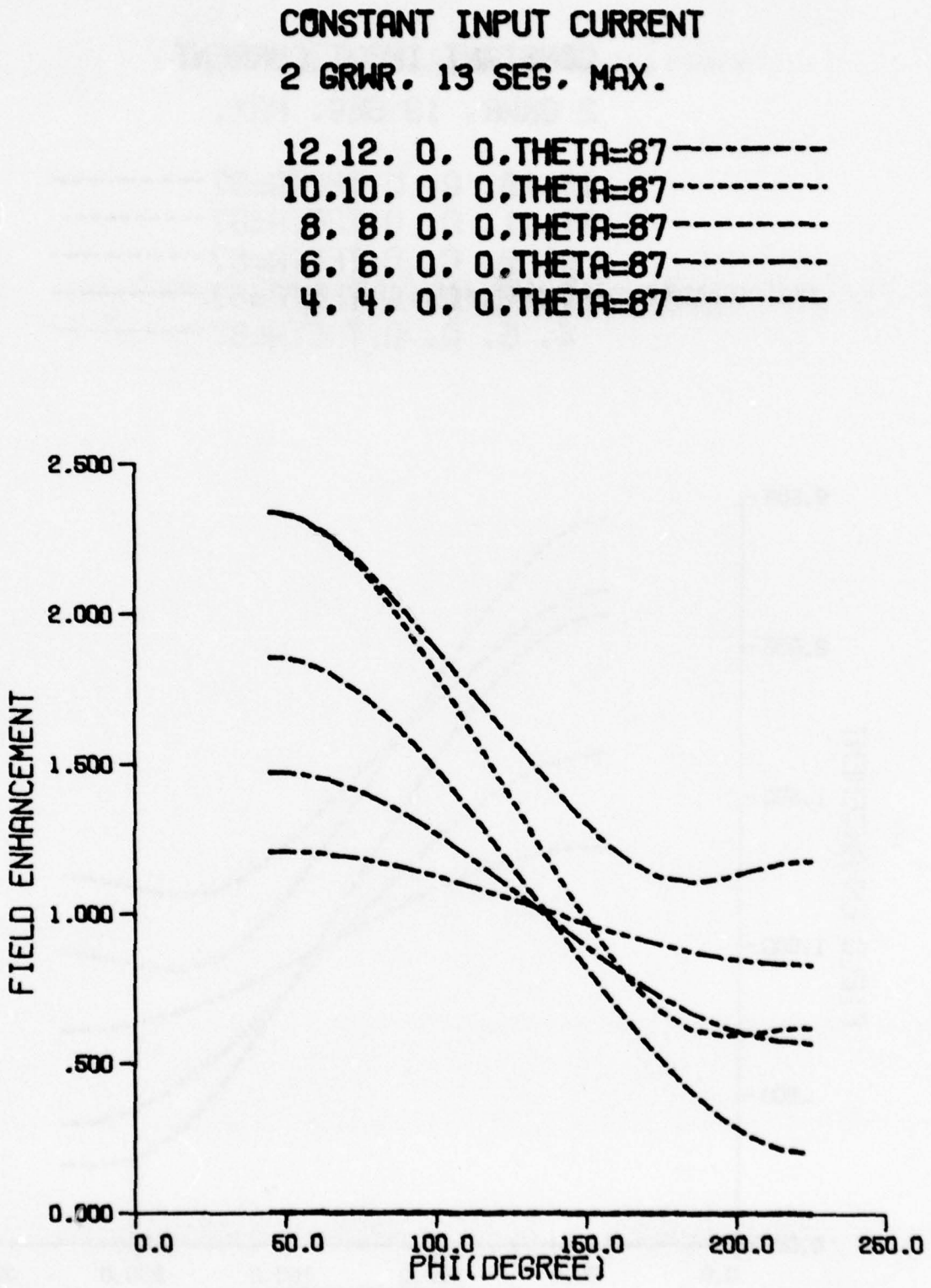

Figure 19a. Low Angle Field Enhancement (θ=87° for a Two-Wire Ground Screen of (N,N, 0, 0) Configuration

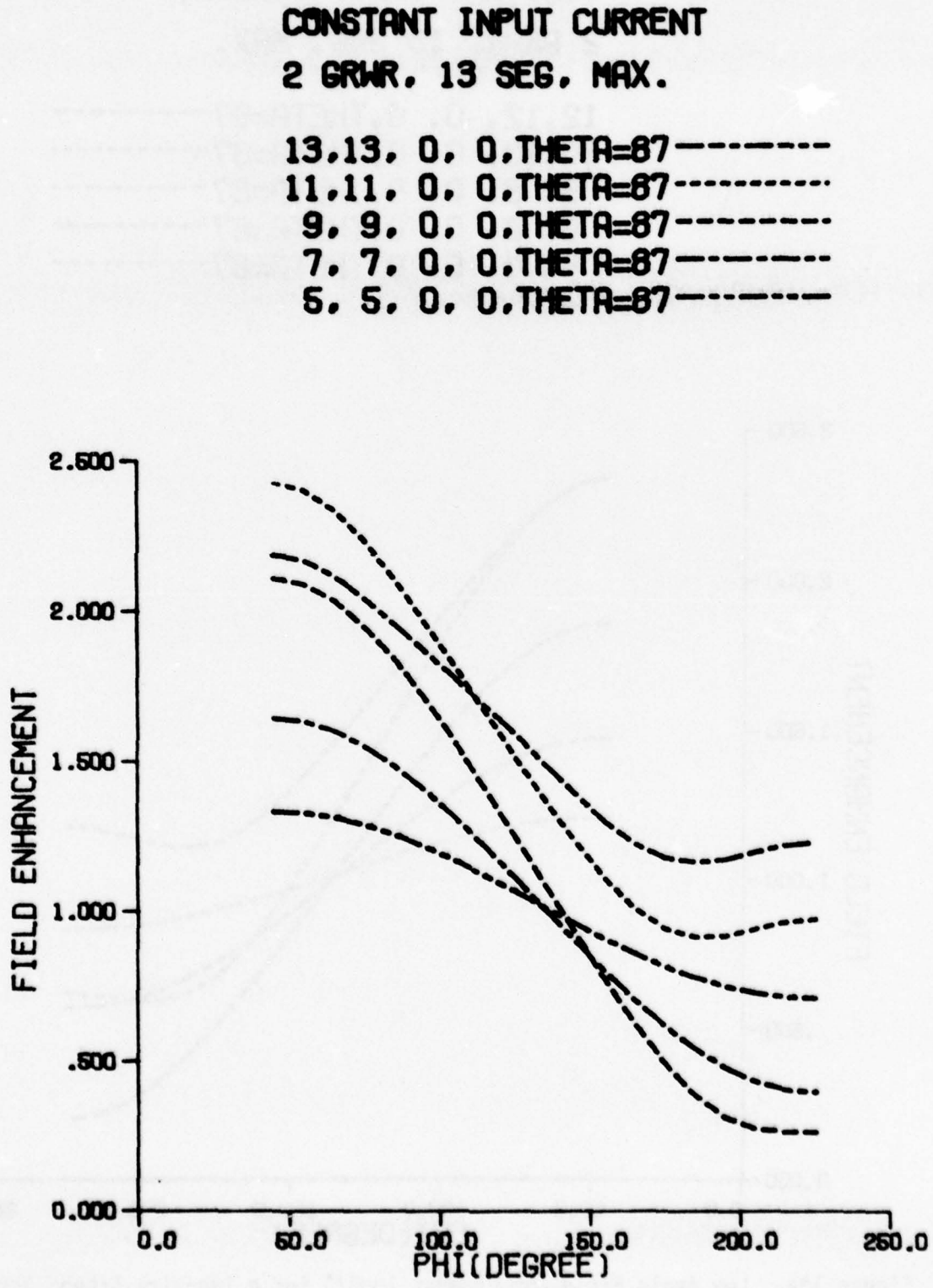

Figure 19b. Low Angle Field Enhancement (θ=87°) for a Two-Wire Ground Screen of (N, N, 0, 0) Configuration

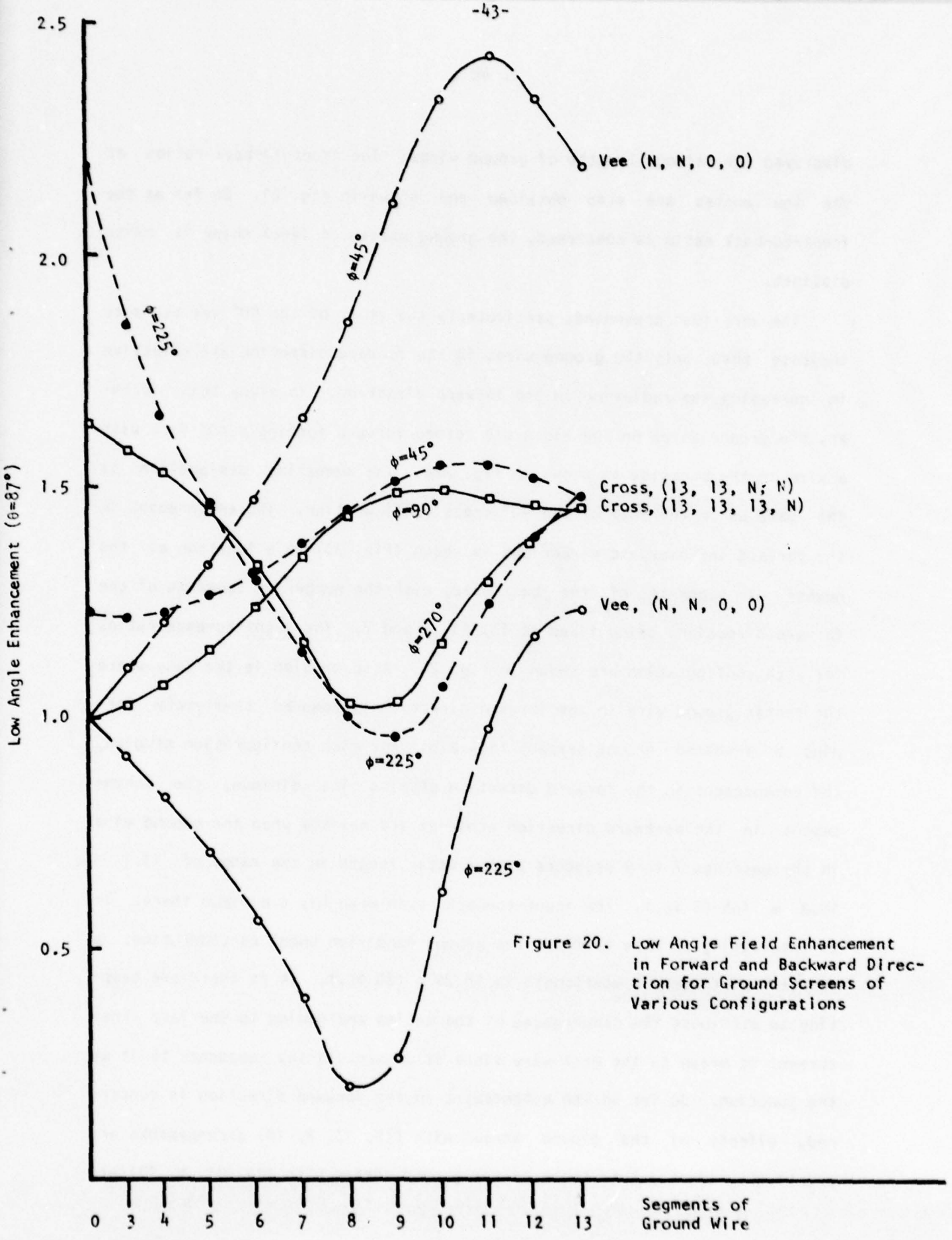

Figure 20. Low Angle Field Enhancement in Forward and Backward Direction for Ground Screens of Various Configurations

displayed for various lengths of ground wires. The front-to-back ratios at the low angles are also obtained and shown in Fig. 21. So far as the front-to-back ratio is concerned, the ground screen of (Vee) shape is quite distinct.

The work just presented, particularly the study of the 90° Vee seems to indicate that only the ground wires in the forward direction are effective in increasing the radiation in the forward direction. To study this further, the ground wires on the sides are folded forward forming a 60° fork with a wire on the backside as shown in Fig. 22a. The numbering designation is the same as in the case of the 90° cross configuration. The enhancement in the forward and backward directions is shown (Fig. 23) as a function of the number of segments of the back wire, with the number of segments of the forward directions being fixed at 13, 11, 9 and 7. The front-to-back ratios for each configuration are shown in Fig. 24. Also studied is the case where the center ground wire in the forward direction is removed completely forming a Y-shaped ground screen, Fig. 22b. For each configuration studied, the enhancement in the forward direction attains its minimum, the enhancement in the backward direction achieves its maximum when the ground wire in the back has 7 to 9 segments with a total length in the range of 13.7 - 19.8 m (45-65 ft.). The front-to-back ratio also has a minimum there. It is interesting to note that for the ground condition under consideration, a quarter of Coleman's wavelength is 18.29 m (60 ft.). It is therefore tempting to attribute the occurrences of the maxima and minima to the fact that current is drawn to the back wire since it presents a low impedance to it at the junction. So far as the enhancement in the forward direction is concerned, effects of the ground screen with (13, 13, N, 13) arrangements are practically identical to those of the ground screen with (11, 11, N, 11) ar-

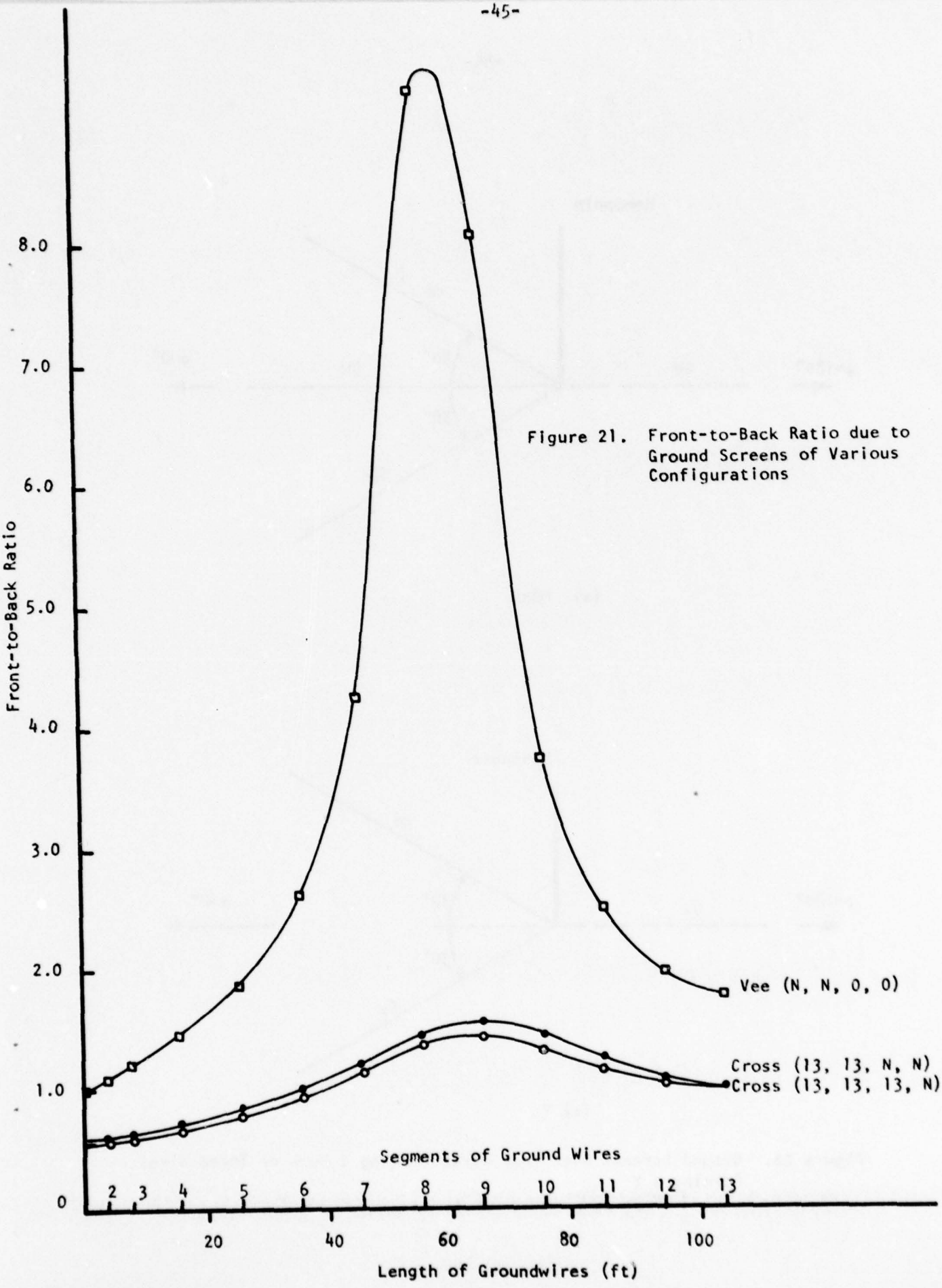

Figure 21. Front-to-Back Ratio due to Ground Screens of Various Configurations

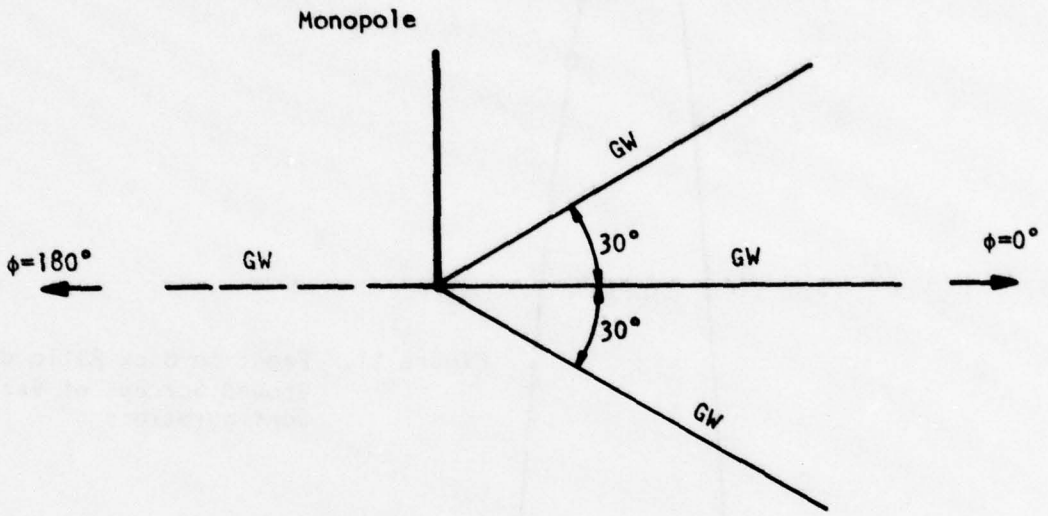

(a) FORK

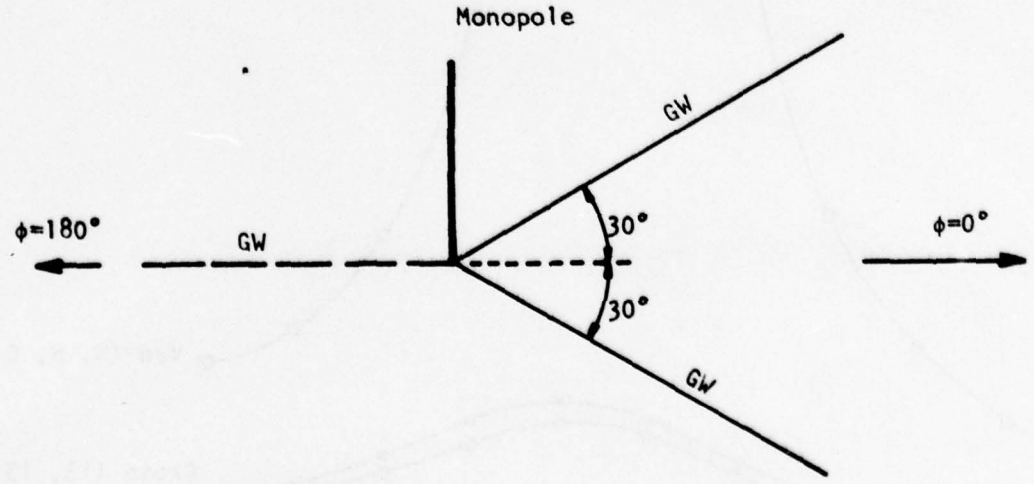

(b) Y

Figure 22. Ground Screens with Four Wires Forming a Fork or Three Wires Forming a Y

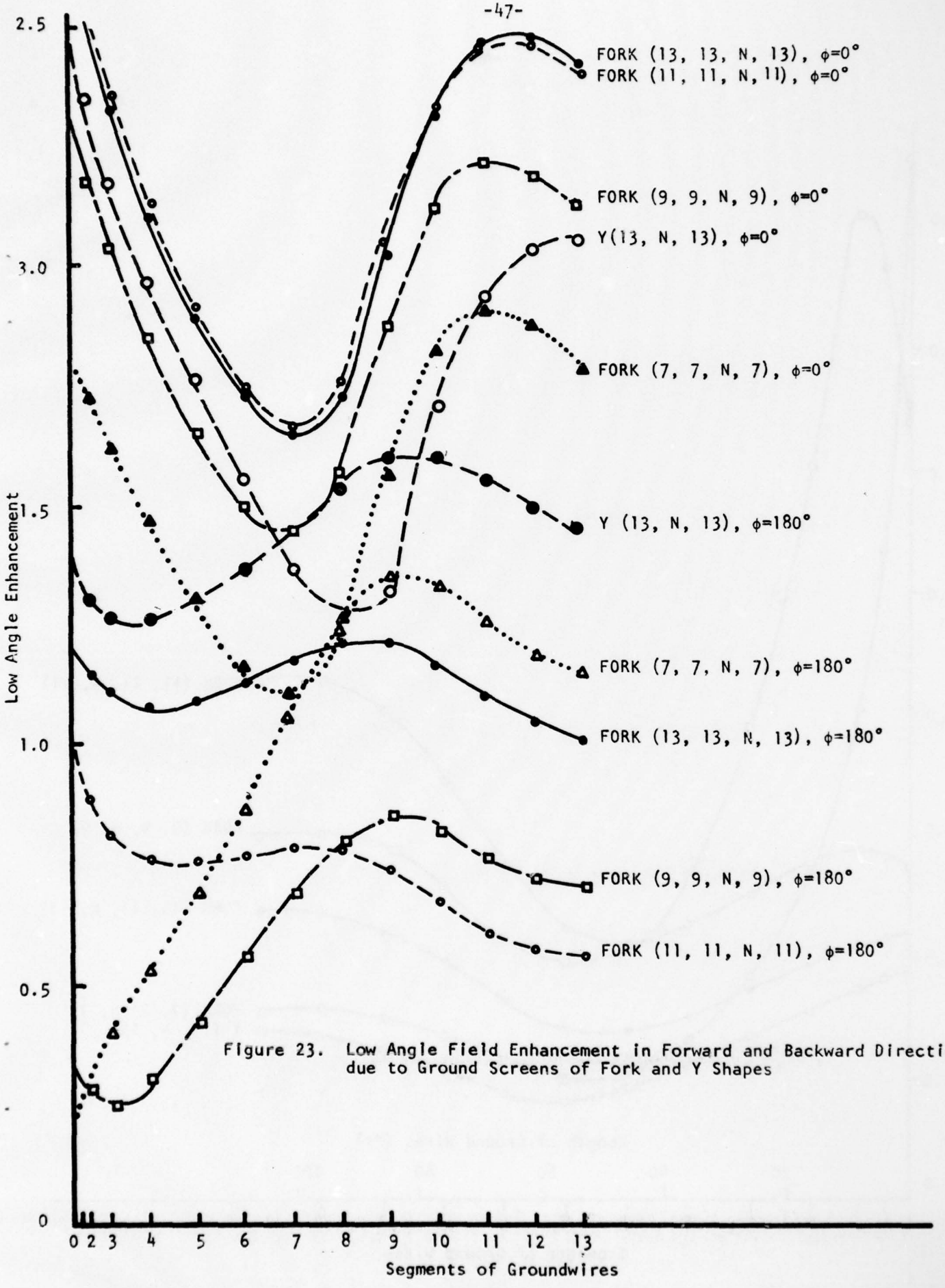

Figure 23. Low Angle Field Enhancement in Forward and Backward Directions due to Ground Screens of Fork and Y Shapes

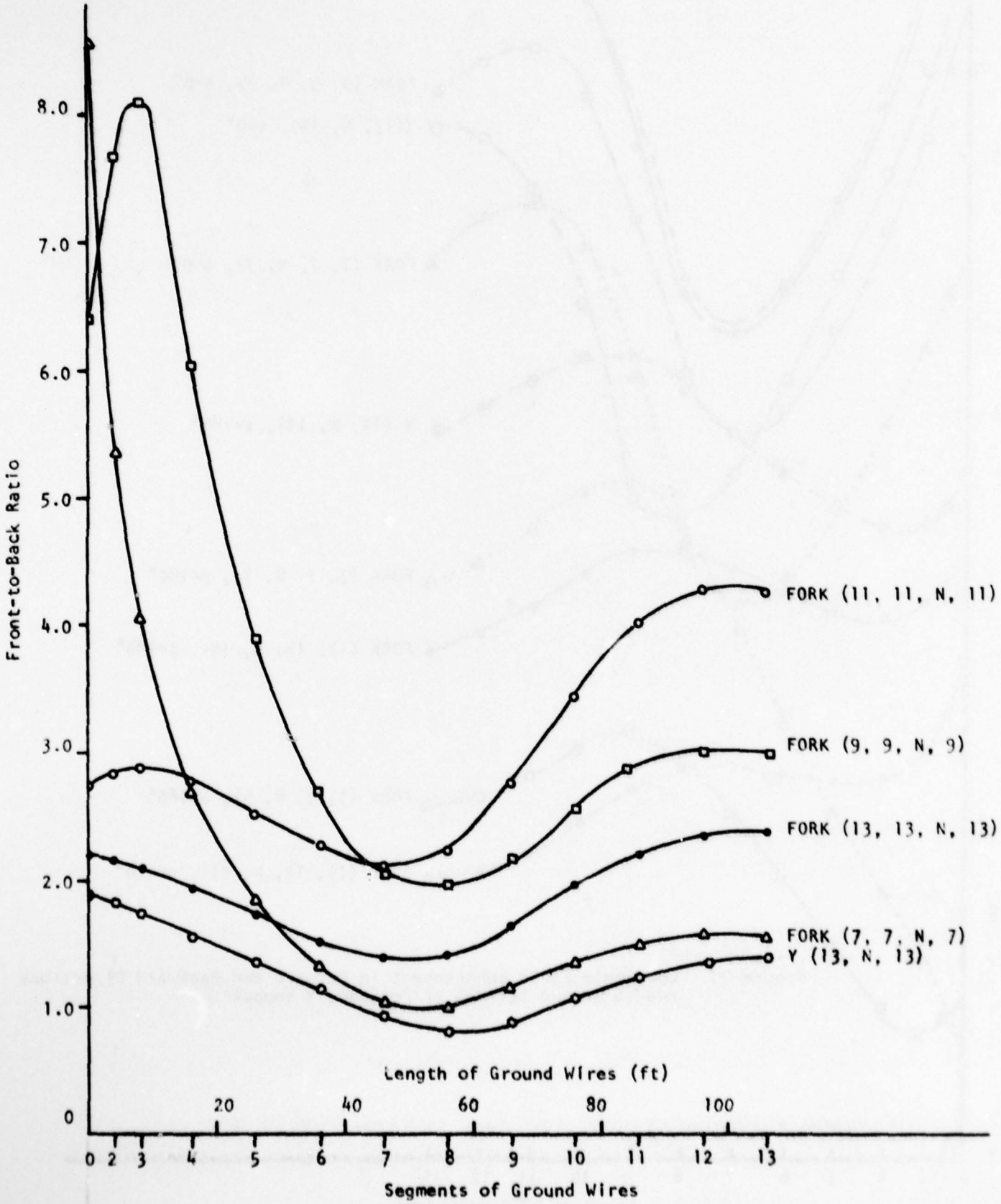

Figure 24. Front-to-Back Ratio Due to Ground Screens of Fork and Y Shapes

rangements. But the front-to-back ratios of the (11, 11, N, 11) arrangements are better than those of (13, 13, N, 13) by 25% to 80%. Thus larger ground screens are not necessarily desirable and certainly not more economical.

7. Effect of the Height of the Backscreen on the Low Angle Radiation

The computer code was also employed in a study whose purpose was to try to minimize the height required for the reflecting screens that are associated with vertically polarized broadside HF antenna arrays. It was assumed that the backscreens were made up of vertical wire elements spaced so as to reflect most of the power. It was desired to reach conclusions applicable to large arrays without actually introducing all of the elements into the computation. Since the effect of the backscreen height is most pronounced in the elevation plane (and since the gain in the horizontal plane is a function of the horizontal extent of the array, which was unspecified), a study was undertaken to determine what might be called a performance unit of the array. The performance unit was to consist of one driven element and the smallest possible number of reflecting wires. A study in which 3, 5 and 7 reflectors of various spacings were employed showed that the results do not change significantly whether there are 5 or 7 reflecting wires spaced at approximately an eighth wavelength from each other. Thus most of the data runs were carried out with 7 reflecting elements.

Cases of different distances between the reflecting elements and the driven element were studied but most of the data on the effect of backscreen size was obtained with a spacing of .125 wavelength between the driven element and the plane of the reflectors. The height of the driven element was slightly under a quarter wavelength at 10 MHz. The height of the elements making up the backscreen was varied systematically from a quarter

wavelength to about a wavelength. The computer program was then asked to compute the radiation pattern (and impedance) of these systems over a lossy ground (ϵ_r = 10, $\sigma = 10^{-3}$mho/m) with a constant power input and to plot the resultant field as a function of the angle θ, measured downward from the zenith. Figs. 25 through 33 show some of the results obtained in this way. The caption on the figures "SEVEN nn+FT REFLECTORS" means that there were seven reflecting elements which were nn feet higher than the quarter-wave driven element. It is interesting to superimpose all of these patterns to see how the results change with reflector height. While there is no substantial difference in the field near the horizon, the height of the peak near $\theta = 60°$ is different and the "sharpness" of the "beam" at the higher angles is dependent on reflector height, with the greatest gain occurring with a reflector height of about 49 feet of extra height, which makes the reflectors about three quarters of a wavelength high. The relative peak value as a function of height is shown in Fig. 34, along with the geometrical arrangements. These data show a broad minimum where the reflector heights are in the neighborhood of one half wavelength, with a sharper peak near three quarters wavelength. Nevertheless, it is noteworthy that even at a reflector height of three fourths of a wavelength, the added gain at the peak is only 5 percent or so greater than that for a reflector height of about one quarter wavelength. And moreover unless the height is made as much as about three quarters, the field is actually reduced when the reflector height is increased from about a quarter wavelength.

8. Conclusion

The effect of simple ground screens on the radiation characteristics of monopoles was studied to help determine the optimal size and shape of ground screens for the enhancement of low angle radiation. Our numerical calcula-

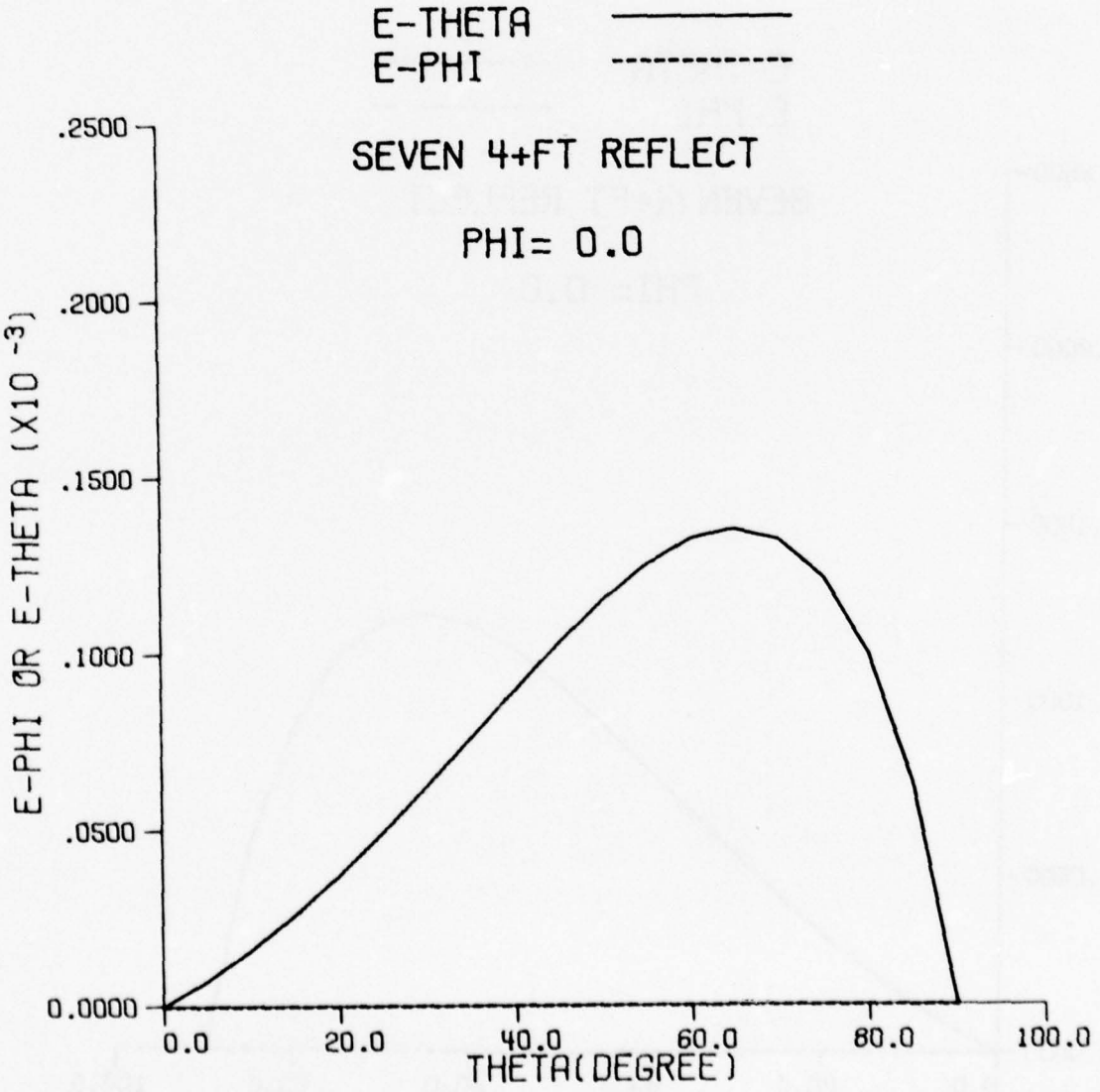

Figure 25. Pattern in forward elevation plane of a driven monopole in front of 7 reflectors, .28 wavelength in height.

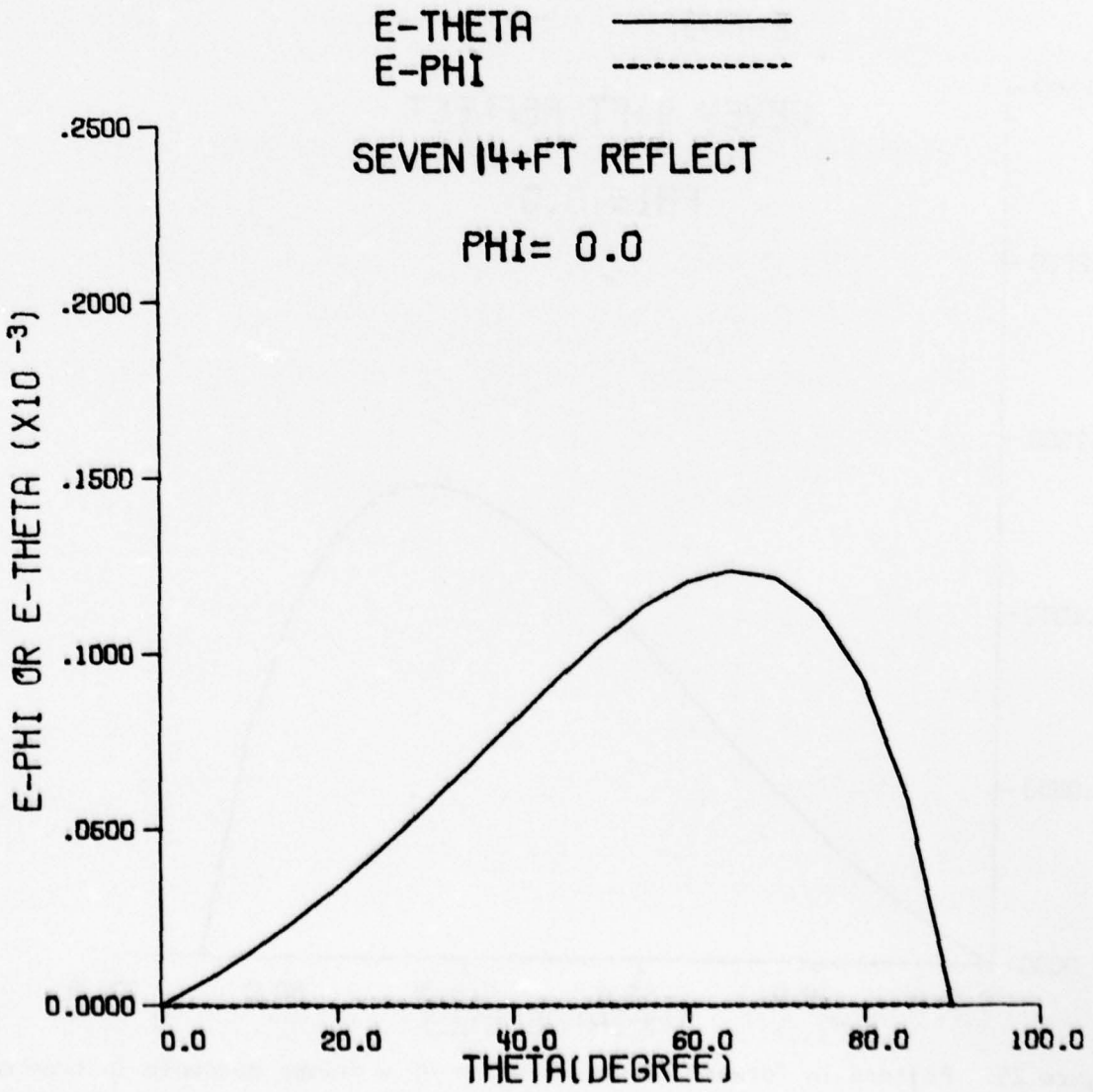

Figure 26. Pattern in forward elevation plane of a driven monopole in front of 7 reflectors, .39 wavelength in height.

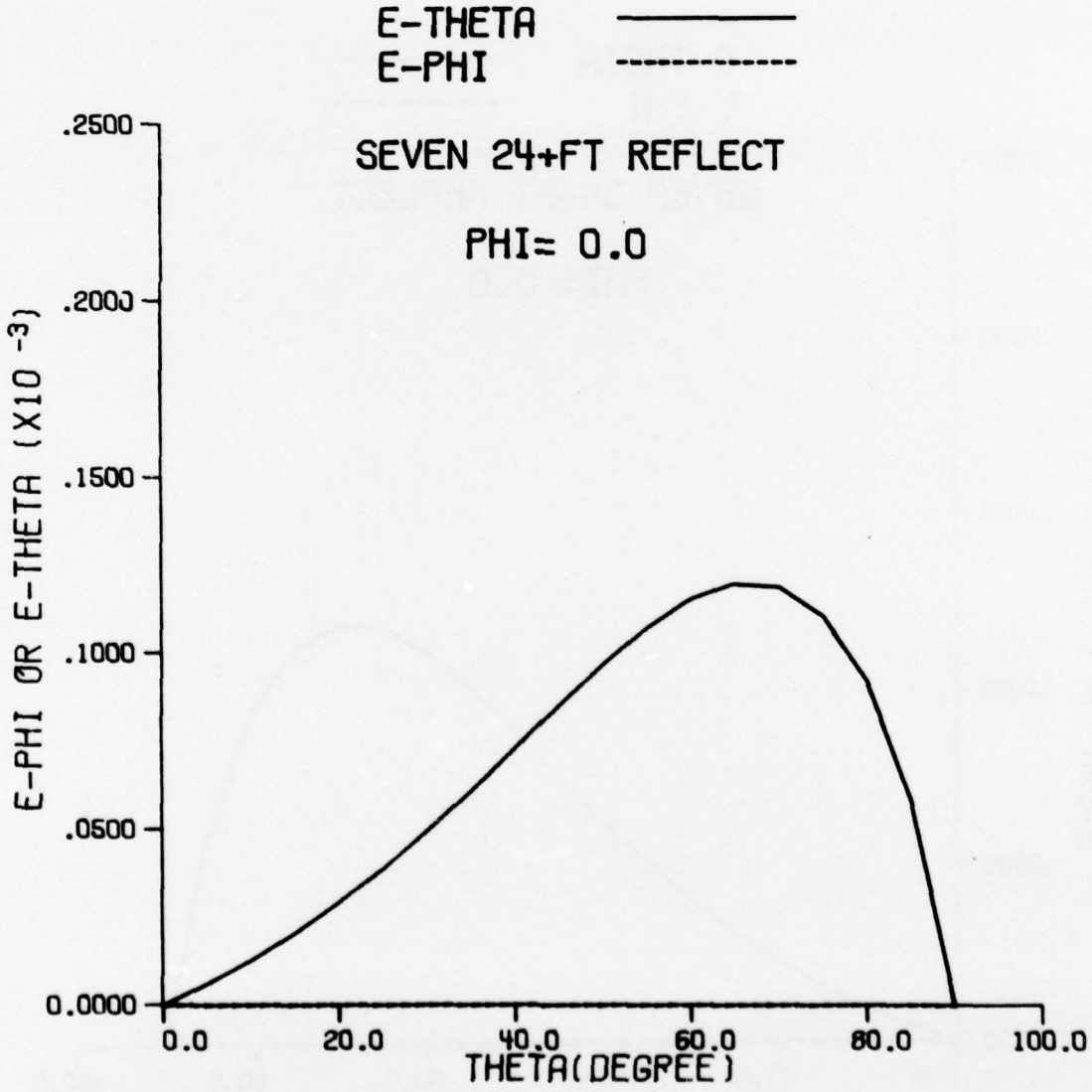

Figure 27. Pattern in forward elevation plane of a driven monopole in front of 7 reflectors, .49 wavelength in height.

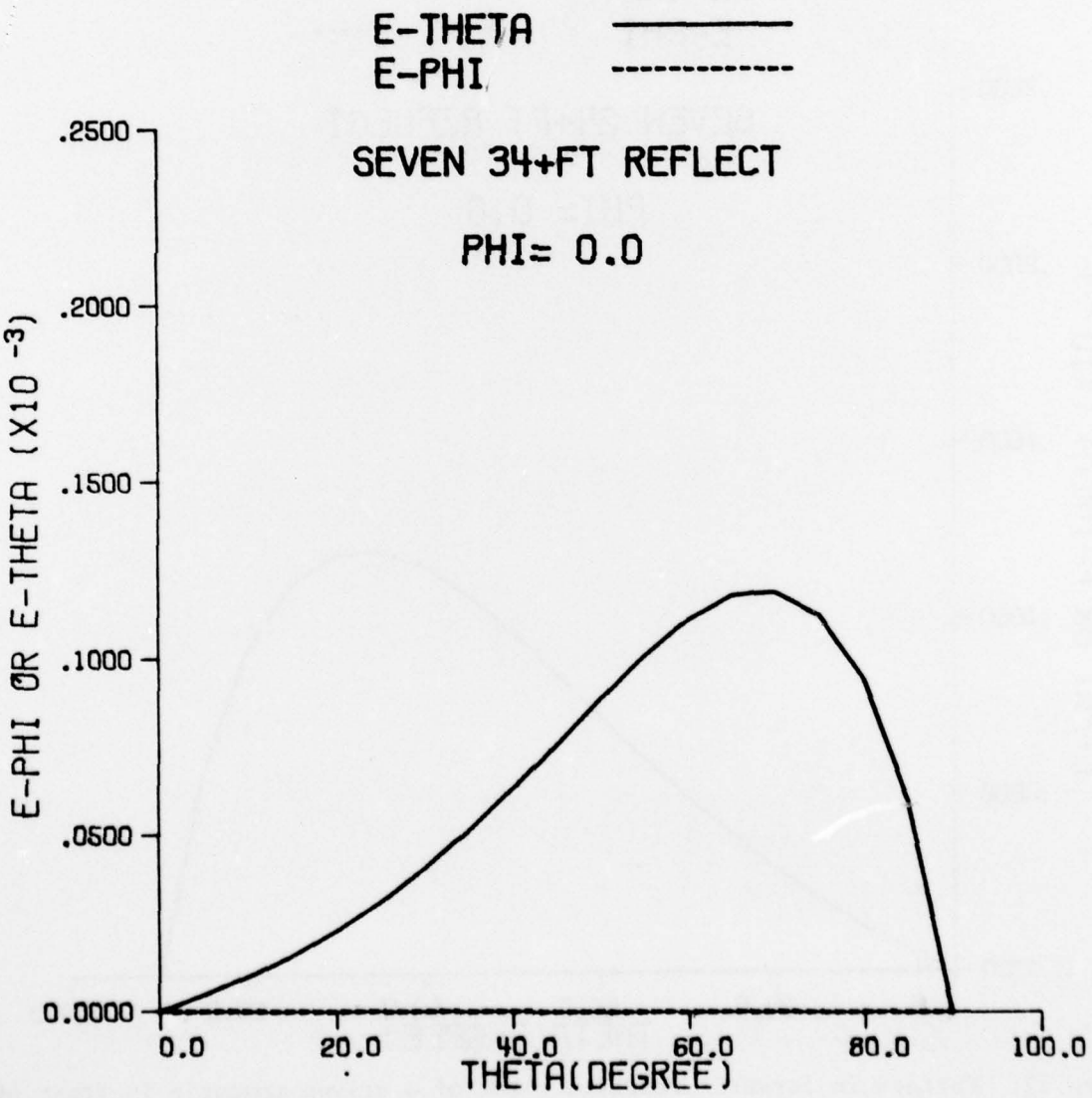

Figure 28. Pattern in forward elevation plane of a driven monopole in front of 7 reflectors, .59 wavelength in height.

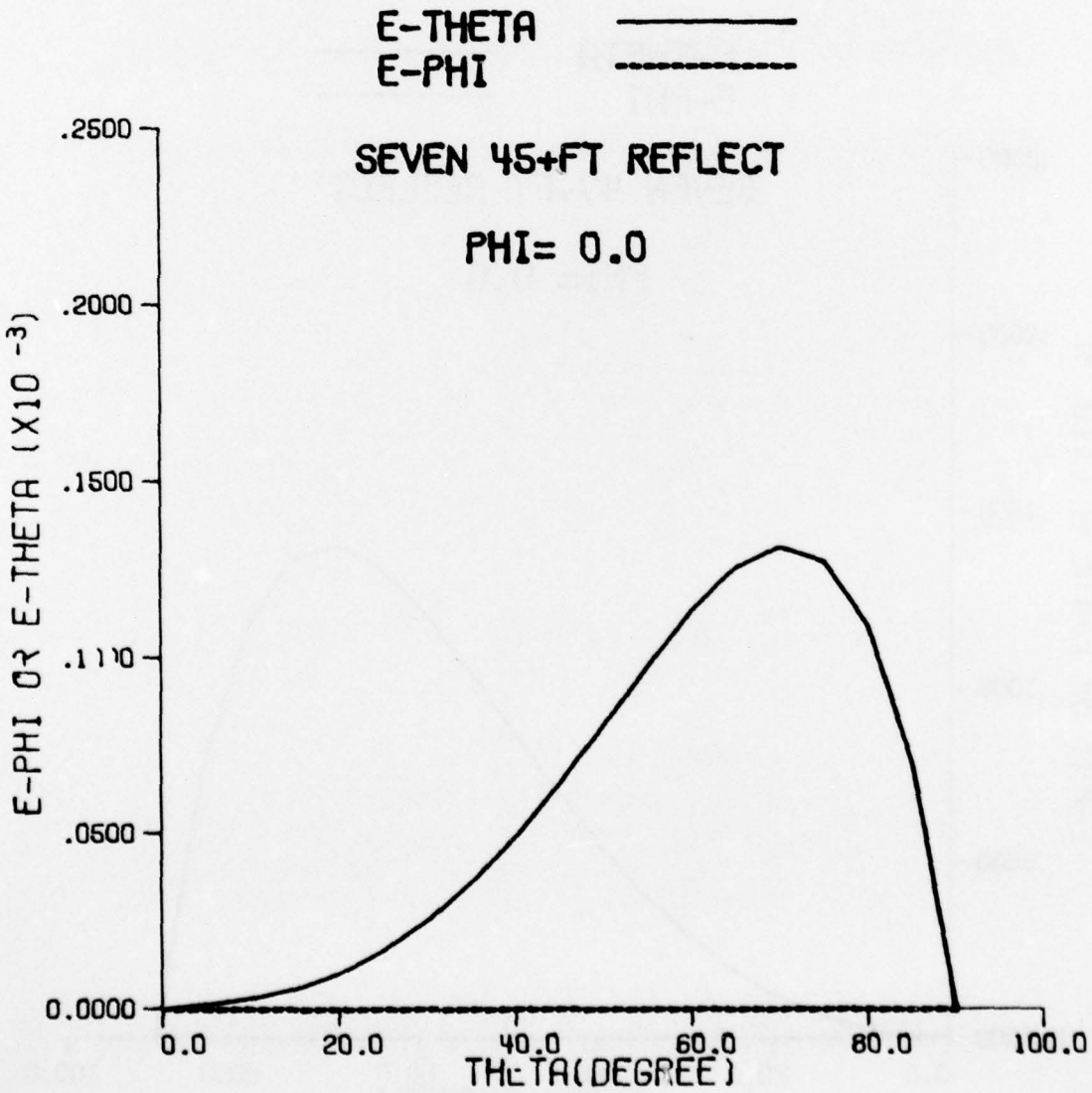

Figure 29. Pattern in forward elevation plane of a driven monopole in front of 7 reflectors, .70 wavelength in height.

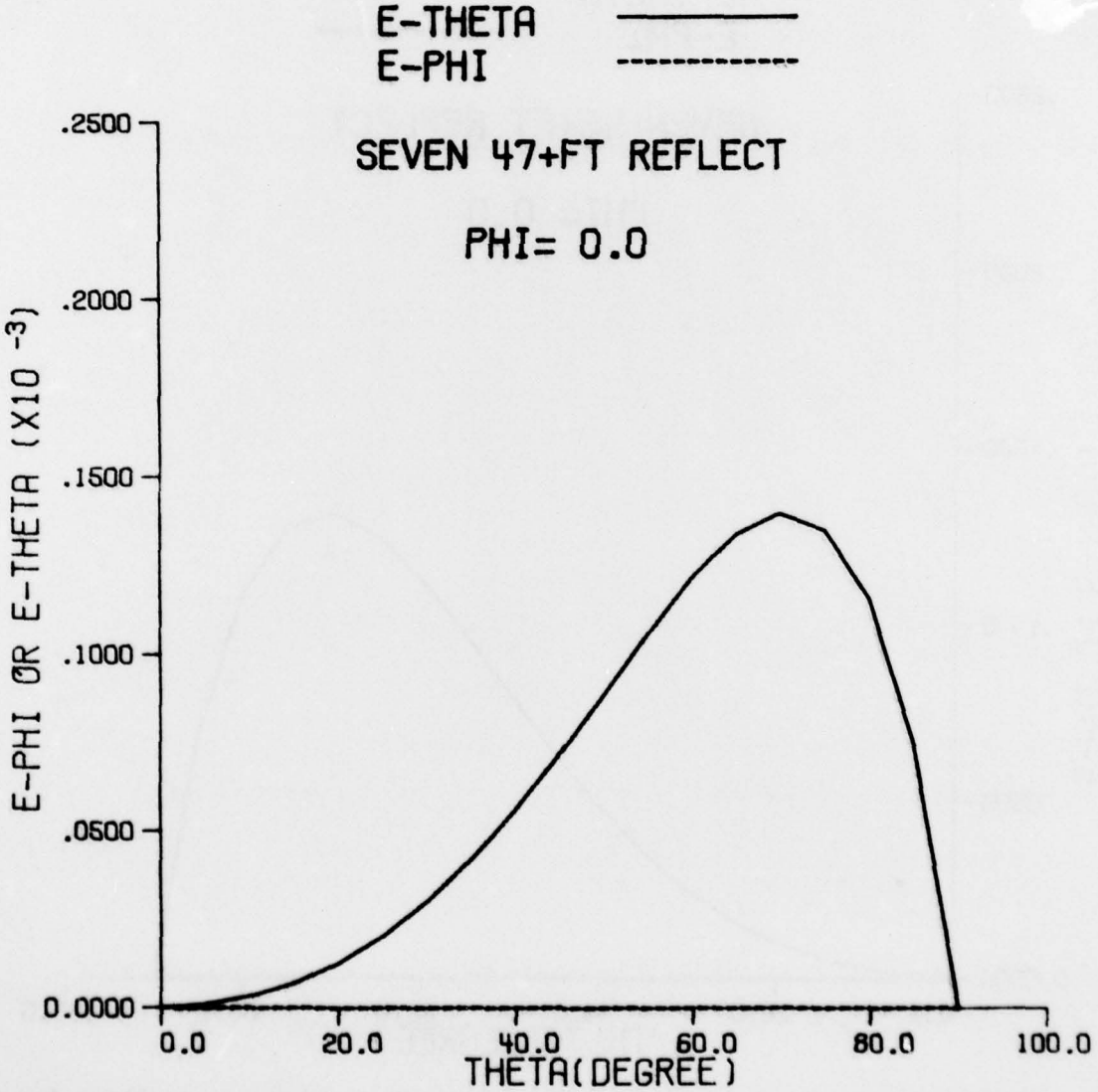

Figure 30. Pattern in forward elevation plane of a driven monopole in front of 7 reflectors, .72 wavelength in height.

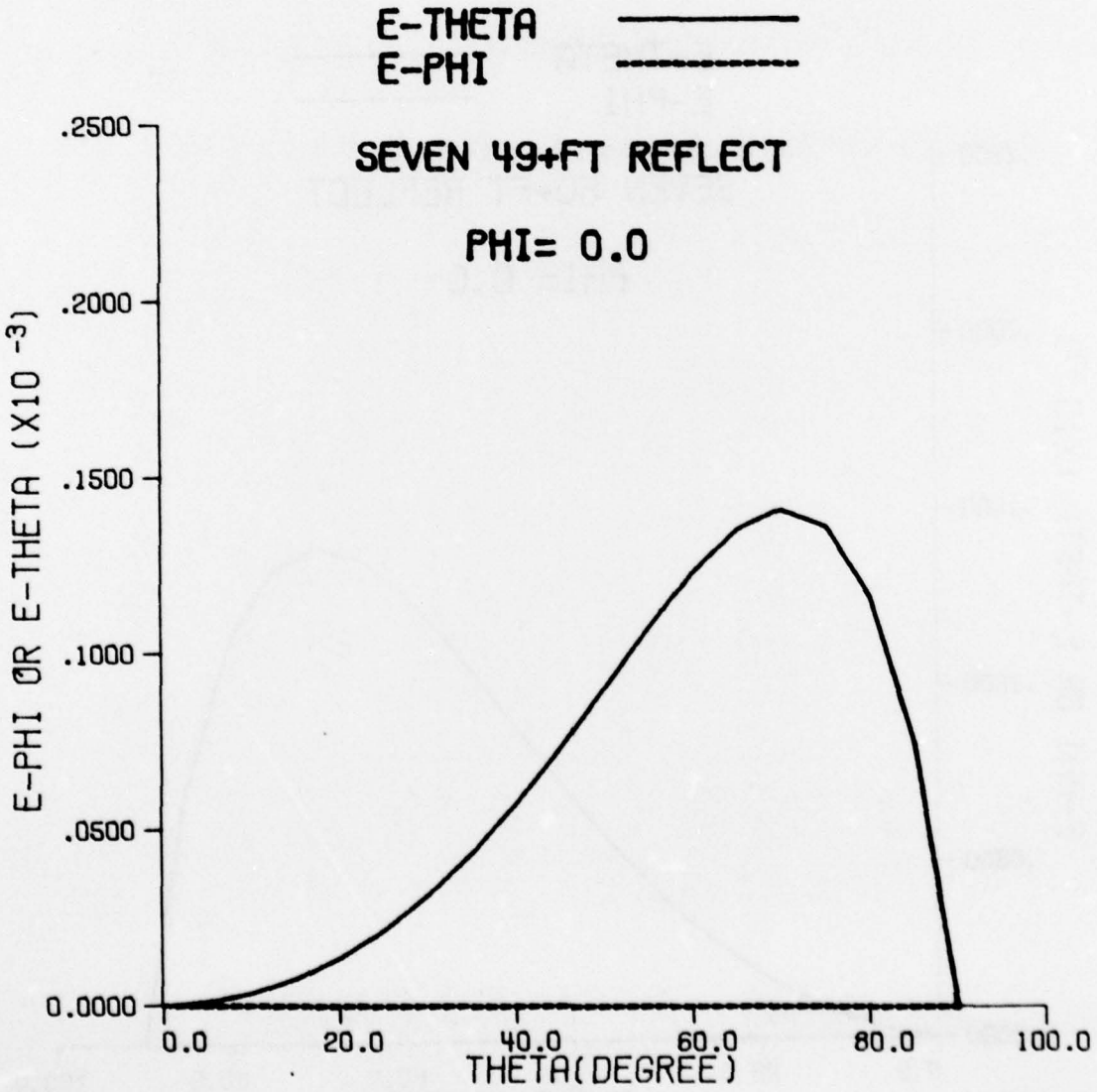

Figure 31. Pattern in forward elevation plane of a driven monopole in front of 7 reflectors, .74 wavelength in height.

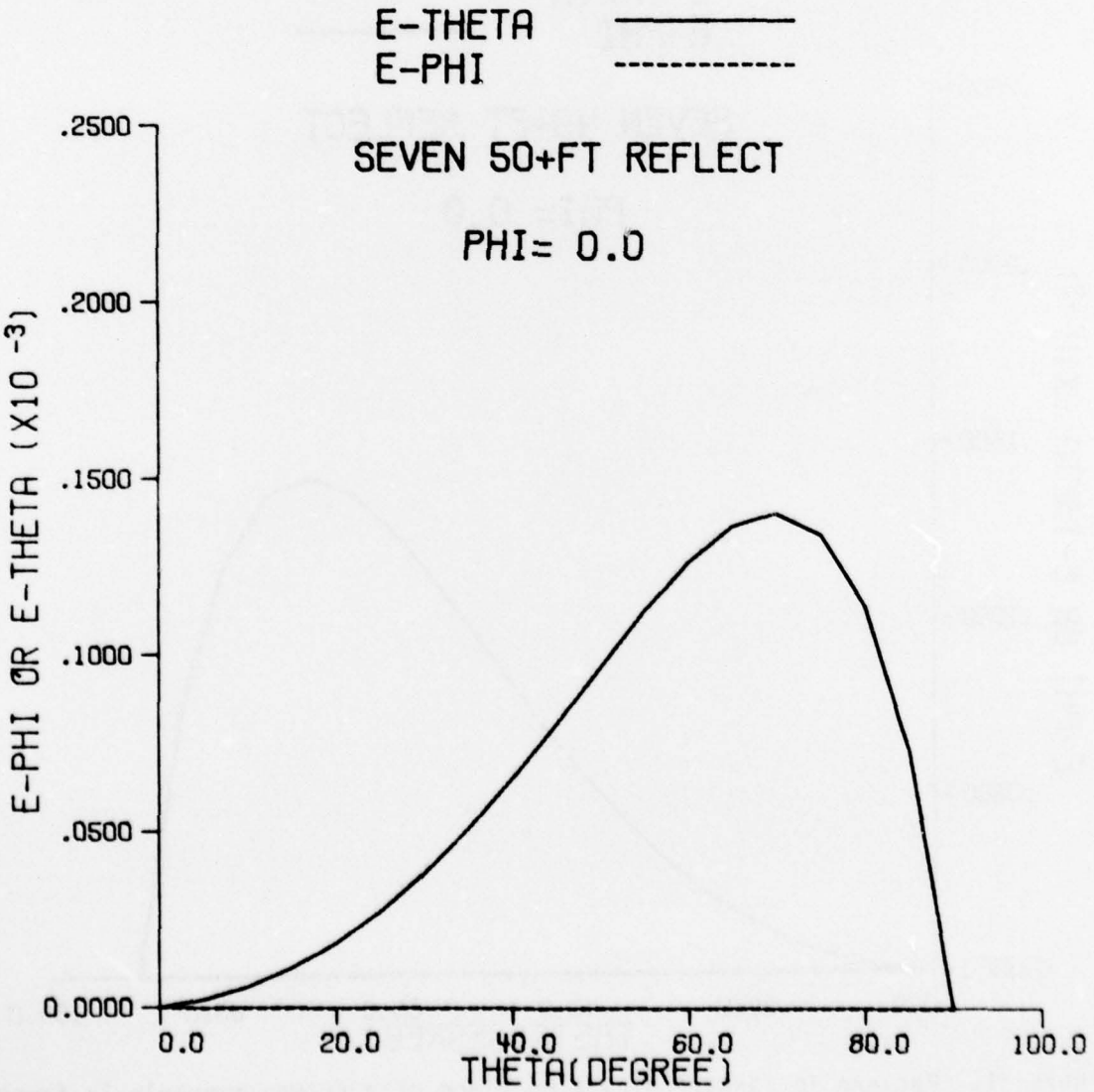

Figure 32. Pattern in forward elevation plane of a driven monopole in front of 7 reflectors, .75 wavelength in height.

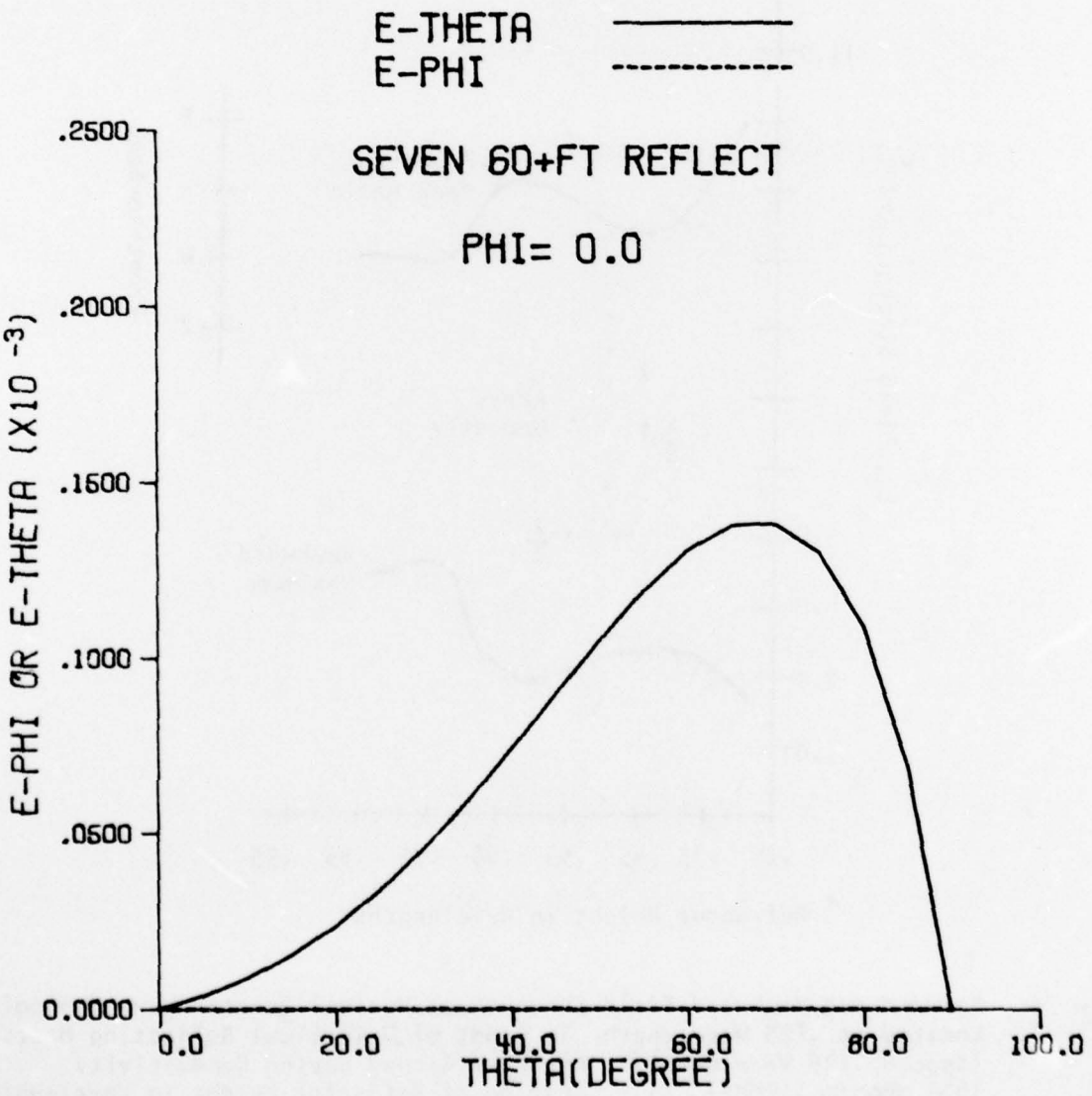

Figure 33. Pattern in forward elevation plane of a driven monopole in front of 7 reflectors, .85 wavelength in height.

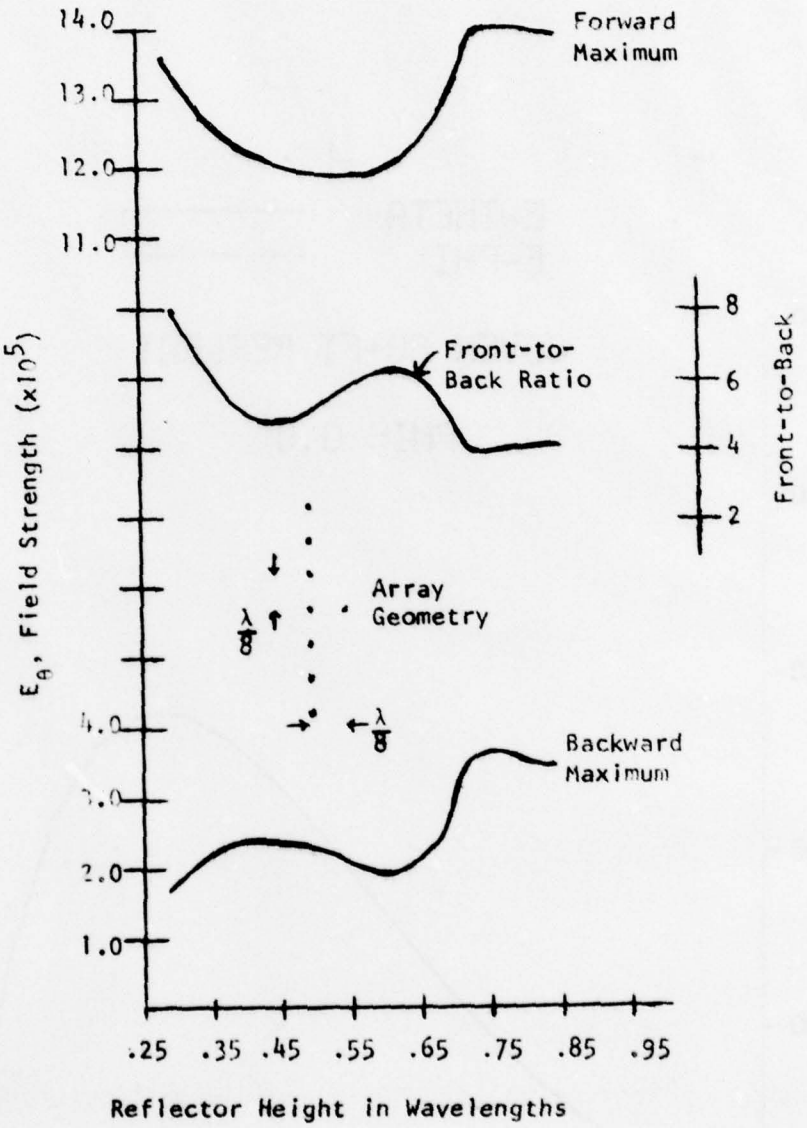

Figure 34. Forward and Backward Field Strength of Nominal Quarter Wave Monopole Located at .125 Wavelength in Front of 7 Vertical Reflecting Masts (Spaced .125 Wavelenth). All Over Ground Having Conductivity 10^{-3} mhos/m (10MHz), as a Function of Reflector Height in Wavelengths.

tion showed that the current induced on a thin ground wire by a neighboring monopole may be approximated by the Coleman's formula with reasonable accuracy. In particular, Coleman's formula may be used in conjunction with elementary transmission line theory as the basis for a crude and simple estimate of desirable lengths of ground wires. In selecting the length of ground wires it is important to draw or to guide the return current toward the forward direction and away from the backward direction. For example, Sec. 5 and 6 of this report show that a short section of a ground wire extended in the backward direction would reduce rather than reinforce the low-angle enhancement in the forward direction, and the low-angle enhancement reaches its minimum when the ground wire is approximately a quarter of Coleman's wavelength.

So far as the backscreens for vertically polarized antenna arrays are concerned, our results show that the height of the vertical elements making up the backscreens should be near an odd number of quarter wavelengths in height, with only small advantage for heights greater than one quarter wavelength.

REFERENCES

1. G. H. Brown, R. F. Lewis and J. Epstein, "Ground systems as a function in antenna efficiency", Proc. IRE, 25, pp. 753-787, 1937.

2. Laport, E. A., Radio Antenna Engineering, McGraw-Hill book Company, Inc. 1952.

3. King, R. W. P., The Theory of Linear Antennas, Harvard University Press, Cambridge, MA, 1956, Chapter VII.

4. Weeks, W. L., Antenna Engineering, McGraw-Hill Book Company, Inc., 1968, Chapter 2.

5. Sommerfeld, A., Partial Differential Equations in Physics, Academic Press, Inc., p. 257, 1949.

6. Lager, D. L., and Lytle, R. J., "Fortran subroutines for the numerical evaluation of Sommerfeld integrals unter anderem", Report UCRL-51821, Lawrence Livermore Laboratory, University of California, Livermore, CA 94550, May 1975.

7. Banos, A. Jr., Dipole Radiation in the Presence of a Conducting Half-Space, Pergamon Press, 1966.

8. King, R. W. P., and Harrison, C. W., Antennas and Waves: A Modern Approach, The M.I.T. Press, 1969, Chapter 14.

9. Wait, J. R., "Characteristics of antennas over lossy earth," Chapter 23 of Antenna Theory, Part II, ed. by R. E. Collin and F. J. Zucker, McGraw Hill Book Company, Inc., 1969.

10. Maley, S. W., R. J. King, and L. R. Branch, "Theoretical calculations of the impedance of a monopole antenna with a radial-wire ground system on an imperfectly conducting half space," Sci. Rept. 26, AFCRL-63-583-PRO-62-201, University of Colorado Contract CST-7429, 1963.

11. Lytle, R. J., and Lager, D. L., "Numerical evaluation of Sommerfeld integrals", Report UCRL-51688, Lawrence Livermore Laboratory, University of California, Livermore, CA, October 1974.

12. Siegel, M. and King, R. W. P., "Electromagnetic fields in a dissipative half-space: A numerical approach", J. Appl. Phys., 41, pp. 2415-2423, 1970.

13. Luke, Y. L., Integrals of Bessel Functions, McGraw-Hill Book Company, Inc., 1962, pp. 246-247.

14. Bannister, P. R., "The quasi-static fields of dipole antennas at the earth's surface", Radio Sciences, 1, pp. 1321-1330, 1966.

15. Bannister, P. R., "The quasi-near fields of dipole antennas", IEEE Transactions on Antennas and Propagation, AP-15, pp. 618-626, 1967.

16. Coleman, B. L., "Propagation of electromagnetic disturbances along a thin-wire in a horizontally stratified medium," Philosophical Magazine, 41, Ser. 7 pp. 276-288, 1950.

17. Chen, C. L. and Weeks, W. L., "Influence of horizontal ground wires on low-angle radiation from HF antennas", Report RADC-TR 77-171, May 1977.

List of Figures

27. Pattern in forward elevation plane of a driven monopole in front of 7 reflectors, .49 wavelength in height.

28. Pattern in forward elevation plane of a driven monopole in front of 7 reflectors, .59 wavelength in height.

29. Pattern in forward elevation plane of a driven monopole in front of 7 reflectors, .70 wavelength in height.

30. Pattern in forward elevation plane of a driven monopole in front of 7 reflectors, .72 wavelength in height.

31. Pattern in forward elevation plane of a driven monopole in front of 7 reflectors, .74 wavelength in height.

32. Pattern in forward elevation plane of a driven monopole in front of 7 reflectors, .75 wavelength in height.

33. Pattern in forward elevation plane of a driven monopole in front of 7 reflectors, .85 wavelength in height.

34. Forward and backward field strength of nominal quarter wave monopole located at .125 wavelength in front of 7 vertical masts (spaced .125 wavelength), all over ground having conductivity 10^{-3} mhos/m (10 MHz) as a function of reflector height in wavelengths.